TENT5 cytoplasmic noncanonical poly(A) polymerases regulate the innate immune response in animals

Vladyslava Liudkovska, Pawel Krawczyk, Aleksandra Brouze, Natalia Gumińska, Tomasz Wegierski, Dominik Cysewski, Zuzanna Mackiewicz, Jonathan Ewbank, Krzysztof Drabikowski, Seweryn Mroczek, et al.

MOLECULAR BIOLOGY

TENT5 cytoplasmic noncanonical poly(A) polymerases regulate the innate immune response in animals

Vladyslava Liudkovska[1,2]†, Paweł S. Krawczyk[1,3]‡, Aleksandra Brouze[1,2]‡, Natalia Gumińska[1], Tomasz Wegierski[1], Dominik Cysewski[3], Zuzanna Mackiewicz[1], Jonathan J. Ewbank[4]§, Krzysztof Drabikowski[3], Seweryn Mroczek[1,2], Andrzej Dziembowski[1,2,3]*

Innate immunity is the first line of host defense against pathogens. Here, through global transcriptome and proteome analyses, we uncover that newly described cytoplasmic poly(A) polymerase TENT-5 (terminal nucleotidyltransferase 5) enhances the expression of secreted innate immunity effector proteins in *Caenorhabditis elegans*. Direct RNA sequencing revealed that multiple mRNAs with signal peptide–encoding sequences have shorter poly(A) tails in *tent-5*–deficient worms. Those mRNAs are translated at the endoplasmic reticulum where a fraction of TENT-5 is present, implying that they represent its direct substrates. Loss of *tent-5* makes worms more susceptible to bacterial infection. Notably, the role of TENT-5 in innate immunity is evolutionarily conserved. Its orthologs, TENT5A and TENT5C, are expressed in macrophages and induced during their activation. Analysis of macrophages devoid of TENT5A/C revealed their role in the regulation of secreted proteins involved in defense response. In summary, our study reveals cytoplasmic polyadenylation to be a previously unknown component of the posttranscriptional regulation of innate immunity in animals.

INTRODUCTION

Innate immunity is an evolutionarily ancient mechanism that provides general host protection against pathogens (*1*). In mammals, innate immunity functions alongside adaptive immunity and also plays a key role in its activation (*2*, *3*). On the other hand, many organisms, including the bacterivore nematode *Caenorhabditis elegans*, lack adaptive immunity and defend themselves solely with innate immune mechanisms (*4*, *5*). Some core components of innate immunity are conserved, but the particular means of protection used by different animals vary. In mammals, the innate system depends on physical and anatomical barriers (e.g., the barrier epithelial cells, mucus, tears, earwax, and stomach acid), the humoral component (i.e., cytokines, chemokines, and defensins secreted by innate immune cells), and several types of phagocytic cells, among them are macrophages, which recognize and destroy pathogens (*6*). *C. elegans* has no specialized immune cells and relies on its barrier tissues, epidermal and intestinal cells, for defense (*4*). An efficient immune response is provided by the high secretion capacity of the particular host cells, as they release a variety of antimicrobial peptides and enzymes that can directly attack pathogens (*4*, *6*). In all organisms studied, the innate immune response is regulated at both the transcriptional and posttranscriptional levels (*4*, *7*). The signaling pathways and transcriptional factors that control innate immunity in worms have been studied in detail, but less is known about the posttranscriptional mechanisms involved in this process.

[1]Laboratory of RNA Biology, International Institute of Molecular and Cell Biology, Trojdena 4, 02-109 Warsaw, Poland. [2]Faculty of Biology, University of Warsaw, Pawinskiego 5a, 02-106 Warsaw, Poland. [3]Institute of Biochemistry and Biophysics, Polish Academy of Sciences, Pawinskiego 5a, 02-106 Warsaw, Poland. [4]Aix Marseille University, INSERM, CNRS, CIML, Turing Centre for Living Systems, Marseille, France.
*Corresponding author. Email: adziembowski@iimcb.gov.pl
†Present address: Laboratory of Stem Cell RNA Metabolism, The International Institute of Molecular Mechanisms and Machines, Polish Academy of Sciences, Smetany 2, 00-783 Warsaw, Poland.
‡These authors contributed equally to this work.
§Present address: European Research Infrastructure on Highly Pathogenic Agents (ERINHA), 98, rue du Trône, Boite 4, Brussels 1050, Belgium.

In eukaryotes, most mRNAs are polyadenylated by the canonical polyadenylate [poly(A)] polymerase during mRNA 3′ end processing in the nucleus (*8*, *9*). The poly(A) tail is essential for mRNA stability, export to the cytoplasm, translation, and turnover (*10*). Poly(A) tails are gradually shortened in the cytoplasm by deadenylases, and their reduction to less than 20 nucleotides (nt) leads to mRNA degradation (*11*). However, in some cases, a poly(A) tail can be extended in the cytoplasm by noncanonical poly(A) polymerases (ncPAPs). These enzymes belong to the family of terminal nucleotidyltransferases (TENTs) and are implicated in a range of physiological processes (*12*–*14*). Cytoplasmic polyadenylation has been mostly studied in the context of the activation of dormant deadenylated mRNAs during gametogenesis (*15*–*17*) and in neuronal processes (*18*, *19*), in which GLD-2 (Germ Line Development 2)/TENT2 polyadenylates certain mRNAs in response to cellular signals. The recent discovery of the TENT5 family of cytoplasmic ncPAPs and the characterization of their functions expanded the repertoire of physiological processes that are affected by this type of posttranscriptional regulation (*20*–*24*). Mammalian genomes encode four TENT5 proteins (TENT5A to TENT5D, also known as FAM46A to FAM46D), all of which are active ncPAPs (*21*, *25*). Functional analysis revealed that TENT5C is a multiple myeloma growth suppressor (*21*, *22*). In multiple myeloma cell lines, TENT5C polyadenylates and stabilizes numerous mRNAs that encode secreted proteins (*21*). TENT5C also plays a crucial role in the regulation of immunoglobulin expression and the humoral immune response in mice through polyadenylation of mRNAs that encode immunoglobulins (*23*, *24*). TENT5A polyadenylates mRNAs encoding collagens and is thus required for the proper bone formation (*26*). However, TENT5 proteins are differentially expressed in mammalian tissues and organs with potential redundancy, which makes study of their functions difficult.

Here, we characterized the only TENT5 family member in *C. elegans*, F55A12.9/PQN-44, which we renamed TENT-5. Transcriptomic and proteomic analysis, along with functional studies, revealed that TENT-5 is an innate immune response regulator. Poly(A) tail profiling by direct RNA sequencing (RNA-seq) showed that TENT-5

polyadenylates and stabilizes mRNAs that encode defense proteins. *tent-5* deficiency led to an impaired innate immune response in worms. The role of TENT5 proteins in innate immunity is evolutionarily conserved because murine macrophages devoid of TENT5A and TENT5C also exhibited defects in polyadenylation of mRNAs that encode proteins with a role in innate immunity. Together, we identified *C. elegans* TENT-5 and its mammalian orthologs TENT5A and TENT5C as previously unknown players that regulate innate host defenses.

RESULTS

TENT-5 is a noncanonical cytoplasmic poly(A) polymerase in worms

In *C. elegans*, there is only one homolog of mammalian TENT5 ncPAPs, PQN-44 (WBGene00004131). Multiple sequence alignment indicated that PQN-44 exhibits high conservation with human TENT5 proteins (fig. S1A) and clusters with the vertebrate TENT5 homologs in phylogenetic analysis (Fig. 1A). Similar to other TENTs, PQN-44 comprises nucleotidyltransferase and poly(A) polymerase–associated domains (fig. S1A). The nucleotidyltransferase domain of TENT-5 contains a well-conserved triad of aspartates/glutamates ([DE]h[DE]h and h[DE]h, with h being a hydrophobic residue) in its catalytic center (fig. S1A) (*12*). These observations suggested that PQN-44 could be a previously unidentified ncPAP in worms; hence, we renamed it TENT-5. To determine whether TENT-5 is an active ncPAP with the potential to polyadenylate substrate mRNAs and enhance their expression, we performed an RNA-tethering assay (*27*), in which TENT-5 is brought to a *Renilla* luciferase (*RL*) reporter mRNA through an artificial interaction (Fig. 1B). 293T cells were cotransfected with the pRL-5Box plasmid, which carries an *RL* containing five boxB sites in its 3′ untranslated region (3′UTR), and construct expressing either wild-type (TENT-5^{WT}) or catalytically inactive [TENT-$5^{D151A, D153A}$ (isoform a)] protein harboring the N-terminal λN boxB-binding domain that ensures interaction with boxB sites. Next, we performed direct full-length RNA-seq (DRS) to measure poly(A) tail length at a genome-wide scale. DRS revealed that tethering of the wild-type TENT-5 led to increased polyadenylation of *RL* mRNA [median poly(A) length of 180 nt], compared to the catalytically inactive TENT-5 [median poly(A) length of 106 nt] (Fig. 1C and fig. S1, B and C). At the same time, the global distribution of transcripts' poly(A) tail lengths was not affected by overexpression of TENT-$5^{WT/MUT}$ (Fig. 1D). Furthermore, the extension of the *RL* poly(A) tail upon tethering of the TENT-5^{WT} resulted in the enhanced production of the reporter protein (fig. S1D), indicating that TENT-5–mediated polyadenylation positively regulates gene expression.

To determine the pattern of TENT-5 expression and its cellular localization, we generated a *tent-5::gfp* knockin strain by CRISPR-Cas9 (fig. S1, E, F, and H). Confocal microscopy revealed that *tent-5* was expressed during all developmental stages, including in embryos and adults (Fig. 1E). Expression was observed in most tissues, including the pharynx, head and tail neurons, seam and hypodermal cells, and intestine (Fig. 1, E and F, and fig. S1G). Notably, TENT-5–green fluorescent protein (GFP) was predominantly localized in the cytoplasm in all cells (Fig. 1, E and F, and fig. S1G). Together, on the basis of the high sequence similarity of TENT-5 with its mammalian counterparts, its polyadenylation activity, and its cytoplasmic localization, we propose that TENT-5 is a novel cytoplasmic ncPAP in worms.

To characterize the role of TENT-5, we used a mutant *tent-5(tm3504)* strain that harbors a deletion that introduces a premature stop codon in *tent-5* (fig. S1H) and produces a reduced level of mRNA predicted to encode a nonfunctional protein (fig. S1I). Using CRISPR-Cas9, we also generated a *tent-5(rtt5)* mutant lacking the entire coding sequence (fig. S1, H and I). Both *tm3504* and *rtt5* are expected to be null alleles. Homozygous mutants carrying these alleles did not, however, display any visible developmental or morphological abnormalities when grown under standard conditions, as revealed by routine observation, measurement of brood size (fig. S1J), and worm body parameters and locomotion analyses (fig. S1, K to N). This observation is in agreement with results from mammals, as *Tent5c* knockout (KO) mice do not display any gross phenotypes (*21*, *23*). We conclude that *tent-5* encodes a poly(A) polymerase that is not essential for worm development under standard conditions.

Loss of *tent-5* leads to the down-regulation of genes that encode innate immune effectors

To gain insight into TENT-5's molecular function, we analyzed the whole transcriptome of age-synchronized L4 worms devoid of *tent-5*. Using RNA-seq, we identified 745 genes differentially expressed in *tent-5(tm3504)* mutant compared to wild-type worms [false discovery rate (FDR) < 0.05] (Fig. 2A and data S1). The expression level of 308 genes was down-regulated and that of 96 genes was up-regulated at least 1.5-fold in mutant animals. The higher number of down-regulated than up-regulated genes in *tent-5(tm3504)* mutant worms is in agreement with our initial hypothesis that polyadenylation by TENT-5 may stabilize mRNAs, and potential direct targets of TENT-5 could be found among the genes which expression is lower in the mutant animals. Clustered Gene Ontology (GO) analysis revealed the association of the down-regulated genes with immune and defense responses, response to biotic stimulus, peptidase and hydrolase activities, lytic vacuole, and extracellular space (Fig. 2B). A substantial number of down-regulated genes encoded various antimicrobial and cytoprotective immune effectors that are constitutively expressed and additionally induced during infection (Fig. 2C). Notably, many of these genes belong to genomic clusters, such as *F55G11.2*, *F55G11.4*, *F55G11.8*, *K02E11.4*, *K02E11.5*, and *K02E11.6*, or to gene families, often linked to innate immunity, including infection response genes (*irg-3*, *irg-5*, and *irg-7*) (*28*), genes that encode caenopores (SPP; 10 genes) (*29*), proteins containing C-type lectin-like domains (CLEC; 10 genes) (*30*), CUB domain containing proteins (7 genes) (*28*), proteins containing the transthyretin-related domain (12 genes) (*31*), collagens (COL; 14 genes) (*31*, *32*), members of the Nematode Specific Peptide family, group C (NSPCs; 10 genes) (*33*), aspartyl proteases (ASP; 10 genes) (*34*), and lysozymes (*lys-7*, *lys-8*, *ilys-5*, and *lys-2*) (*35*). Tissue enrichment analysis (TEA) of down-regulated genes indicated, among other terms, their association with the intestine (Fig. 2D and fig. S2A). In worms, the intestine has a prominent role in innate immunity, as intestinal cells secrete antimicrobial peptides and digestive enzymes into the gut lumen (*4*, *35*, *36*).

Although GO term analysis of the up-regulated genes also revealed their connection with the immune response and intestine, only a few of them encoded the immune effector proteins (*gst-13*, *asp-10*, *clec-187*, *clec-265*, *clec-42*, *dod-22*, *fipr-22*, *lys-4*, *ftn-2*, *hrg-3*, *math-38*, *K08D8.4*, *ZK228.4*, *C37A5.3*, and *F31F7.1*) (data S1). Among the genes up-regulated in mutant worms were also three genes belonging to a single operon (CEOP4272) and encoding mitogen-activated protein kinase homologs essential for innate immune response—*pmk-1*, *pmk-2*, and *pmk-3* (*4*). This observation is important as it may suggest the compensatory effect of signaling pathways in *tent-5(tm3504)*

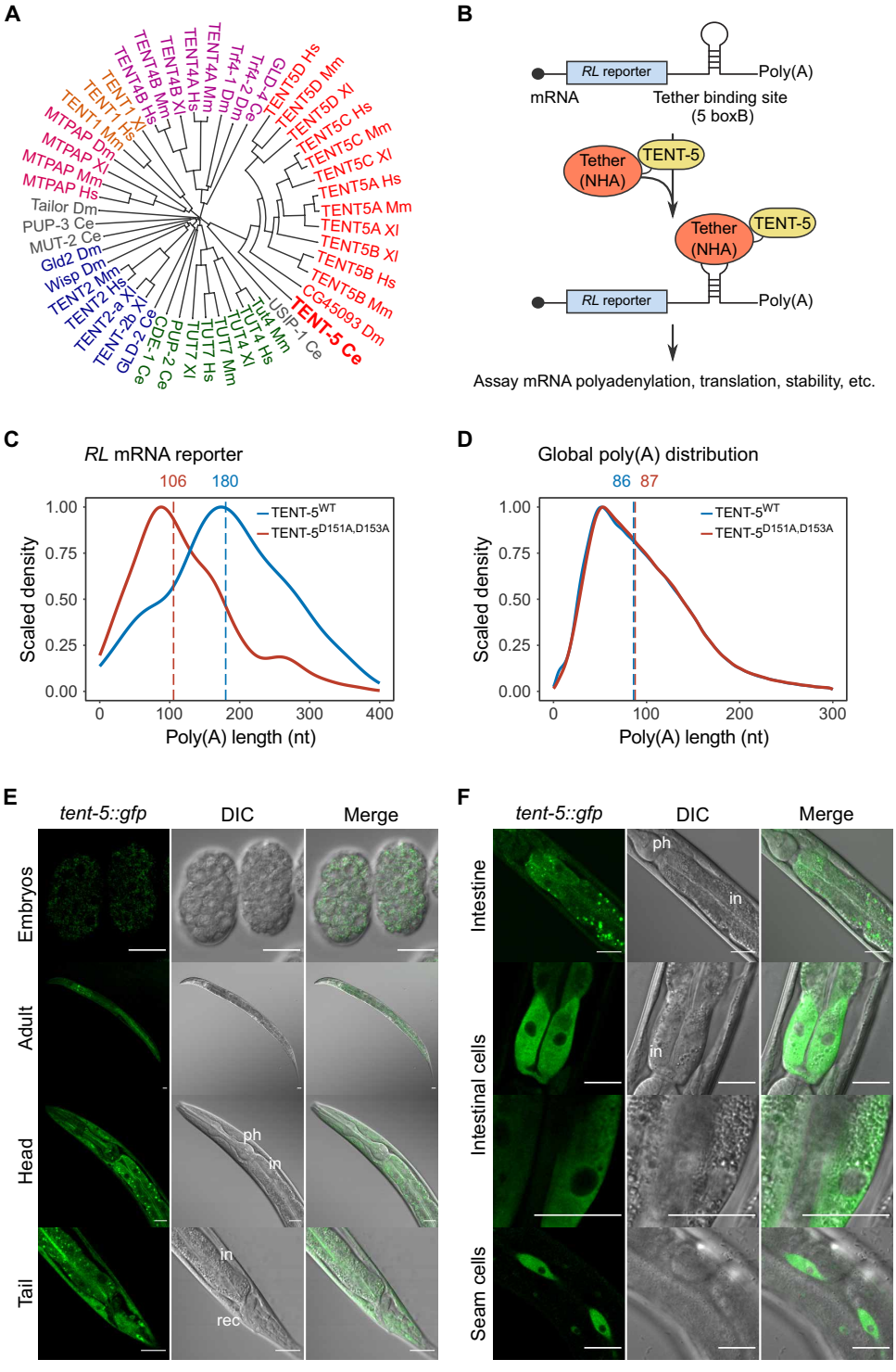

Fig. 1. TENT-5 is a noncanonical cytoplasmic poly(A) polymerase in worms. (**A**) Phylogenetic relationship among 48 TENTs from five model organisms (Hs, *Homo sapiens*; Mm, *Mus musculus*; Xl, *Xenopus laevis*; Dm, *Drosophila melanogaster*; Ce, *C. elegans*). (**B**) Schematic illustration of RNA tethering assay, modified from (*27*). A protein of interest (TENT-5$^{WT/D151A,D153A}$) binds to a *RL* reporter mRNA through an artificial protein-RNA interaction (tether). For tethering assays described in this work, 293T cells were cotransfected with a construct that expresses *RL*, containing a tether binding site (five boxB sites) in its 3′UTR, and a construct expressing either wild-type or catalytically inactive TENT-5 harboring the N-terminal λN boxB-binding domain and an HA-tag (NHA). (**C** and **D**) DRS-based poly(A) length profiling of mRNA following tethering assay. Tethering of wild-type TENT-5 led to increased polyadenylation of an *RL* reporter mRNA compared to a tethering with a catalytically inactive TENT-5^{D151A,D153A} mutant. Shown are density distribution plots for *RL* mRNA (C) and all other transcripts detected in 293T cells (D) scaled to 1. Vertical dashed lines represent median poly(A) lengths (in nucleotides). (**E** and **F**) Representative fluorescence and differential interference contrast (DIC) microscopy images of TENT-5–GFP expression in embryos and adult *tent-5::gfp* knockin worms (*tent-5(rtt6[tent-5::gfp::3xflag] I)*. ph, pharynx; in, intestine; rec, rectum. Scale bars, 20 μm.

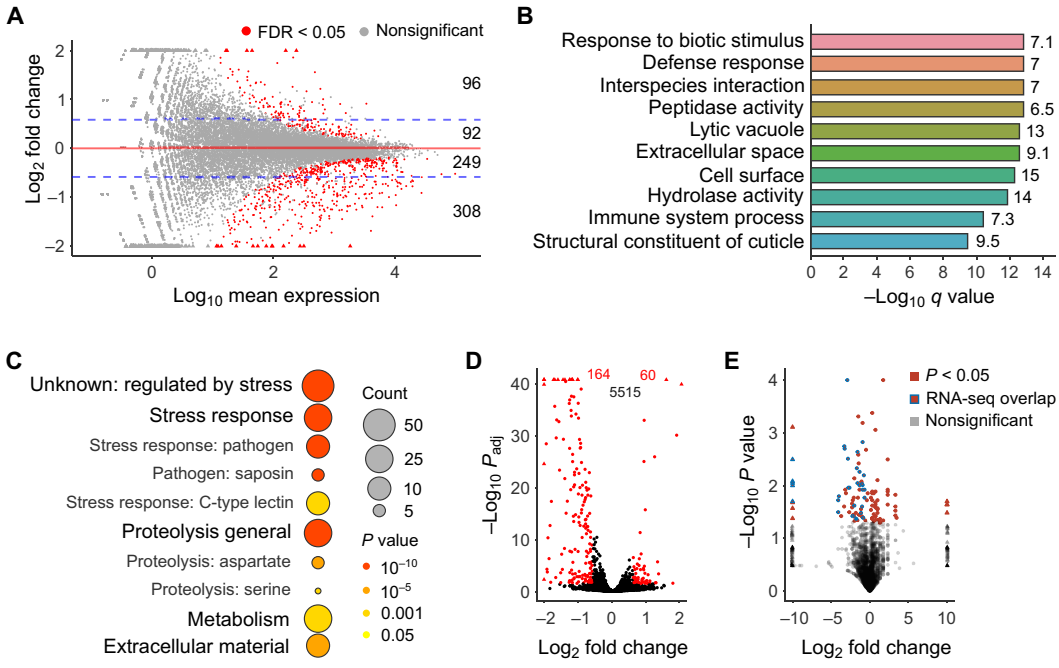

Fig. 2. Loss of *tent-5* leads to the down-regulation of genes that encode innate immune effectors. (**A**) MA plot illustrates differential gene expression in *tent-5(tm3504)* mutant compared to the wild-type worms. Statistically significant values (FDR < 0.05) are shown in red. Blue dashed lines mark the threshold of the $\log_2(1.5)$ fold change. Numbers on the right indicate the number of genes differentially expressed for each fold change group. Triangles, here and (D) and (E), represent data points outside the axes limits. (**B**) Overrepresented functional GO terms of genes down-regulated [$\log_2$FC ($\log_2$ fold change) < $-\log_2(1.5)$] in *tent-5(tm3504)* mutant in comparison to the wild type. Numbers on the right indicate the enrichment fold change for each term. (**C**) WormCat visualization of categories enriched in genes down-regulated 1.5-fold or more in *tent-5(tm3504)* worms. Results are presented as scaled heatmap bubble charts, where the color signifies *P* values and the size specifies the number of genes in each category. (**D**) In the RNA-seq dataset, 5739 genes are associated with the "intestine" GO term cellular compartment (WBbt:0005772). From genes down-regulated or up-regulated in mutant worms at least 1.5-fold (A), 164 and 60 genes are associated with this GO term, respectively. Statistically significant values (FDR < 0.05) are shown in red and nonsignificant in black ($n = 5515$). (**E**) Volcano plot showing proteins, which abundance was significantly changed in mutant (red shapes, $n = 114$). Red shapes with blue borders represent a common part with RNA-seq results ($n = 33$).

mutant to counteract the lower expression level of numerous immune effectors or may point out some nondirect processes connected to the *tent-5* loss. There are no up-regulated genes statistically significantly enriched for the "extracellular region" GO term.

To check whether deregulation of mRNA levels in mutant worms correlated with changes in protein abundance, we performed a large-scale semiquantitative proteomic analysis comparing extracts from L4-stage wild-type and *tent-5(tm3504)* mutant animals. Among proteins with significantly changed abundance ($P < 0.05$), we identified 67 proteins with decreased levels in *tent-5*–deficient worms (Fig. 2E and data S2). Overall, the results of the proteomic analysis were in agreement with the transcriptomic data (Fig. 2E). Notably, some proteins from the defense-associated families mentioned above were less abundant in mutant worms (e.g., three CLEC, three COL, two SPP, two ASP, and two LYS; data S2), and this was mirrored in a more general enrichment for proteins with described or putative roles in innate immunity, as well as protein catabolic processes (fig. S2B). Furthermore, proteins with a decreased level in mutant worms were associated with the intestine (fig. S2C), again in agreement with the transcriptomic analysis.

Consistent with the role of TENT-5 ncPAP in the immune response, the expression of *tent-5* was induced approximately twofold upon the infection with *Staphylococcus aureus*, as revealed by reverse transcription quantitative polymerase chain reaction (RT-qPCR) analysis (Fig. 3A and fig. S3A), in line with previously published datasets (*37*, *38*). To explore further the function of TENT-5 in the immune response, we checked whether immune- and stress-related genes were deregulated in *tent-5(tm3504)* mutants in comparison to wild-type worms after 8 hours of infection with *S. aureus*. RNA-seq results showed that 296 genes were down-regulated 1.5-fold or more (FDR < 0.05) (Fig. 3B and data S3). More than half of all genes for which expression was down-regulated in *tent-5(tm3504)* mutant worms grown on *Escherichia coli* HB101 were also down-regulated in wild-type worms upon infection (Fig. 3C). In agreement with this, results of the GO analysis and TEA were comparable between both datasets and showed that most down-regulated genes were potentially involved in innate immunity (fig. S3, B and C). TENT-5 was necessary for the proper expression of immune genes in both infected and noninfected animals (fig. S3D). Furthermore, the genes down-regulated in *tent-5*–deficient worms are known to be regulated by a variety of pathways (*28*, *36*, *37*, *39*–*43*), indicating that TENT-5's action is not limited to a single signal transduction pathway. Note that some of the 62 genes whose expression was up-regulated in *tent-5*–deficient worms at least 1.5-fold were associated with a defense response (*pmk-1*, *pmk-2*, *pmk-3*, *lys-10*, *ilys-2*, *zip-10*, *clec-60*, *clec-86*, *fbxa-60*, *fbxa-105*, *C10C5.2*, *K08D8.4*, *M04C3.2*, and *C49G7.10*) (data S3). However, their overlap with genes up-regulated in mutant worms grown on *E. coli* HB101 was quite limited (14%). Again, this might suggest that up-regulation of gene expression may be a mainly secondary effect.

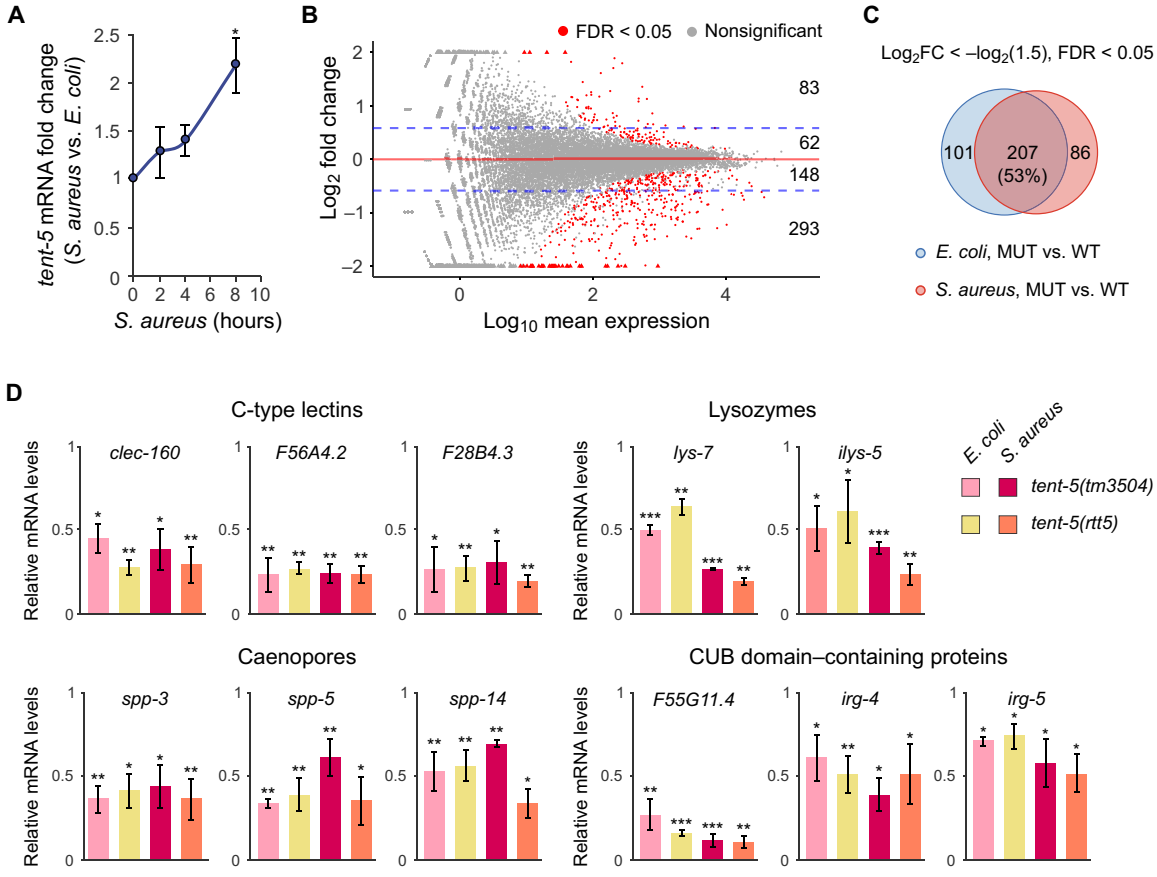

Fig. 3. TENT-5 deficiency leads to the down-regulation of genes that encode innate immune effectors. (**A**) RT-qPCR illustrating the induction of *tent-5* expression in the wild-type worms challenged with *S. aureus* at the time point. Relative *tent-5* mRNA level was normalized to *act-1* and uninfected animals. Data represent means ± SD of three biological replicates; $^{*}P \leq 0.05$ (one-tailed *t* test). (**B**) MA plot showing differential expression of genes in *tent-5(tm3504)* mutant compared to wild type upon infection of L4 worms with *S. aureus* for 8 hours. Plot description as in Fig. 2A. (**C**) Venn diagrams demonstrating the overlap between genes differentially expressed in tent-5–deficient worms grown on nonpathogenic *E. coli* and upon infection by *S. aureus* (FDR < 0.05). MUT, mutant; WT, wild type. (**D**) RT-qPCR analysis of relative levels of mRNA expression in *tent-5(tm3504)* and CRISPR-Cas9–generated *tent-5(rtt5)* mutant grown on *E. coli* or exposed to *S. aureus* for 8 hours. Relative abundance of mRNAs was normalized to *act-1* and wild type. Data represent means ± SD of three biological replicates; $^{*}P \leq 0.05$, $^{**}P \leq 0.01$, and $^{***}P \leq 0.001$ (two-tailed *t* test).

To validate the observed molecular phenotypes of the *tent-5(tm3504)* strain, we grouped down-regulated genes into several functional categories or families and verified their expression in infected and noninfected *tent-5(rtt5)* mutant animals using the RT-qPCR analysis. The results for *tent-5(rtt5)* recapitulated those of *tent-5(tm3504)* strain, with the null mutant exhibiting a down-regulation of expression for all transcripts tested (Fig. 3D and fig. S3E). Thus, we conclude that the observed gene expression changes were due to TENT-5 deficiency. Together, the results of the global transcriptomic and proteomic analyses indicate that TENT-5 is involved in the innate immune response by controlling the expression of immune genes regulated by several signaling pathways.

TENT-5 is required for the host defense against various bacterial strains

The results of the global transcriptomic analysis strongly suggested that TENT-5 could be directly involved in the regulation of genes influencing the interaction between *C. elegans* and bacteria, including many encoding secreted proteins with antimicrobial activity. When *tent-5* mutant worms were grown on *E. coli* HB101, they exhibited a slightly shorter survival than the wild type when grown at both 20°C (Fig. 4A) and 25°C (Fig. 4B). *E. coli* is not a natural food source for *C. elegans* and, under standard culture conditions, is mildly pathogenic to adult worms (*35*, *44*, *45*). To check the possibility that mutants have a shorter life span due to the pathogenesis of *E. coli*, we tested the survival of worms fed on either ultraviolet (UV)– or heat-killed *E. coli* in comparison to the intact bacteria. *tent-5*–deficient mutants exhibited survival curves more comparable to the wild-type worms when cultured on dead bacteria (fig. S4, A to D), indicating that the survival defect of mutant worms could result from their compromised immunity. We then monitored the survival of wild-type and *tent-5*–deficient worms infected with *S. aureus*, *Pseudomonas aeruginosa*, *Serratia marcescens*, and *Photorhabdus luminescens*. These bacterial pathogens colonize the worm's intestinal lumen, causing intestinal distention and worms' death within 3 to 10 days (*46*–*48*). The *tent-5*–deficient mutants were significantly more susceptible to the infection than the wild type (Fig. 4, D and E, and fig. S4, E to G). To investigate whether there are differences in the accumulation of *E. coli* HB101 and *P. aeruginosa* PAO1 in the intestines of wild-type and mutant worms, we performed colony-forming unit (CFU) assays (*49*, *50*). We observed that *tent-5*–deficient worms had higher bacterial load in their guts compared to

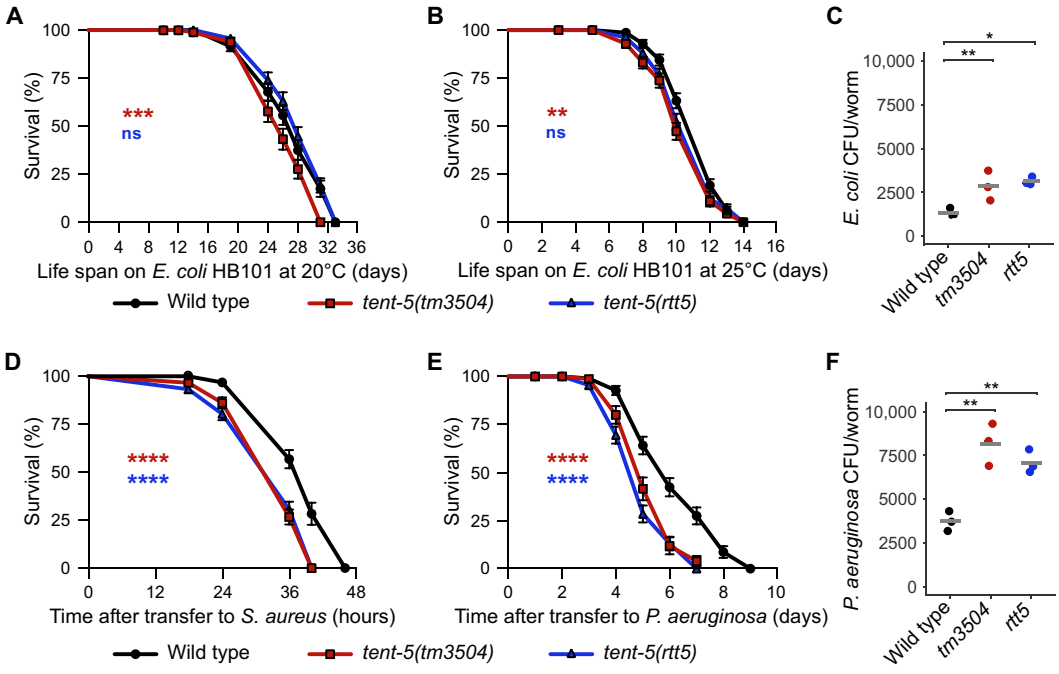

Fig. 4. TENT-5 is required for the host defense against various bacterial strains. Survival of wild-type, *tent-5(tm3504)*, and *tent-5(rtt5)* mutant worms grown on non-pathogenic *E. coli* HB101 at 20°C (**A**) and 25°C (**B**) or infected with *S. aureus* (**D**) and *P. aeruginosa* PAO1 (**E**). For survival on *P. aeruginosa* and *E. coli*, nematode growth medium (NGM) plates contained FUdR. Experiments are representative of three independent trials; $^{**}P < 0.01$, $^{***}P < 0.001$, and $^{****}P < 0.0001$; ns, not significant (log-rank test). Survival data can be found in table S1. Intestinal accumulation of *E. coli* HB101 (**C**) and *P. aeruginosa* (**F**) was measured on the 5th and 4th days of adulthood, respectively. The number of viable internal bacteria in worms' gut is shown in CFU per animal. Points show values for experimental biological replicates calculated as a mean of at least two technical replicas. Line denotes the average value for biological replicates. $^{*}P \leq 0.05$ and $^{**}P \leq 0.01$ (two-tailed *t* test).

the wild type (Fig. 4, C and F). The observed effects indicate that TENT-5 is important for the defense against a range of Gram-positive and Gram-negative pathogens, which use different infection strategies and induce different but overlapping host gene expression responses (*31*, *34*, *46*, *51*). Notably, the localization of TENT-5–GFP in the cytoplasm of the intestinal cells (Fig. 1F) is in agreement with its role in the regulation of innate immune genes, as many immune genes down-regulated in mutant worms are expressed in this tissue (fig. S2, A and C, and data S1 and S2). Together with the observation that *tent-5* mutants are less resistant to infection with several pathogenic bacteria, our results support the hypothesis that TENT-5 plays an important role during host defense and also suggest that TENT-5 may contribute to the regulation of longevity or general fitness in *C. elegans*.

Transcripts down-regulated in the *tent-5*–deficient mutants are direct targets for polyadenylation by TENT-5

To elucidate the mechanism by which TENT-5 regulates innate immunity in worms, we first explored the possibility that TENT-5 might regulate one or more transcription factors responsible for the expression of immune genes (*4*). However, we did not identify any transcription factors among the genes down-regulated in *tent-5(tm3504)* animals or transcriptional repressors among the up-regulated ones (data S1). As a cytoplasmic poly(A) polymerase, TENT-5 would be predicted to have a stabilizing effect on mRNAs by extending their poly(A) tails. We thus hypothesized that transcripts down-regulated in *tent-5* mutants might be direct targets for polyadenylation by TENT-5. To identify mRNAs that may be subjected to TENT-5 polyadenylation, we performed genome-wide poly(A) tail profiling in *tent-5(tm3504)* and wild-type age-synchronized L4 worms using Oxford Nanopore DRS (fig. S5A), which we have previously implemented to find substrates of TENT5C and TENT5A in B cells and osteoblasts, respectively (*23*, *26*). We obtained in total ~12 million transcriptome-wide reads from two wild-type and two mutant biological replicas, of which 70% passed quality control and were used for the analysis of the poly(A) tail lengths (data S4) and differential expression of genes (data S5). The expression levels of identified transcripts were in strong agreement with Illumina RNA-seq results, providing additional confidence in data quality (fig. S5B). Moreover, GO analysis of genes for which expression levels were down-regulated at least 1.5-fold in *tent-5(tm3504)* mutant worms (FDR < 0.05) (data S5) revealed their association with the immune response (fig. S5C), again recapitulating observations obtained by standard RNA-seq (Fig. 2B and data S5).

The distribution of the global poly(A) tail lengths was consistent with the previous reports (Fig. 5A) (*52*, *53*). It has been shown that in adult worms, highly expressed housekeeping transcripts show negative correlation between their poly(A) tail length and mRNA levels (*52*, *53*). Accordingly, we found that genes with highly expressed mRNA tended to have slightly shorter median poly(A) tail length than the ones with medium and low expression levels (fig. S5D), with this trend being particularly evident for the highly expressed transcripts encoding ribosomal proteins (fig. S5E). However, such a trend does not undermine the crucial role of poly(A) tail length in regulating mRNA stability. It rather supports the notion that different functional groups of mRNAs might have various determinates of their stability with varying effects of poly(A) tail length compared to other features, such as ribosome association or sequence motives.

We found 96 mRNAs that had a median poly(A) tail length that was at least 5 nt shorter in the *tent-5*–deficient worms (FDR < 0.05) compared to the wild-type animals (Fig. 5B and data S4). At the same time, we observed no changes in the mRNA polyadenylation between mutant and wild type for the transcripts encoding components of the translational apparatus (Fig. 5C) and other transcripts, which are routinely used as references in high-throughput studies (fig. S5F) (*54*). Almost 70% of these mRNAs were also down-regulated at least 1.5-fold in *tent-5(tm3504)*, according to both RNA-seq and DRS (fig. S5G), implying that they represent the direct substrates for polyadenylation by TENT-5 in wild-type animals. Next, we analyzed the relationship between the median poly(A) tail length

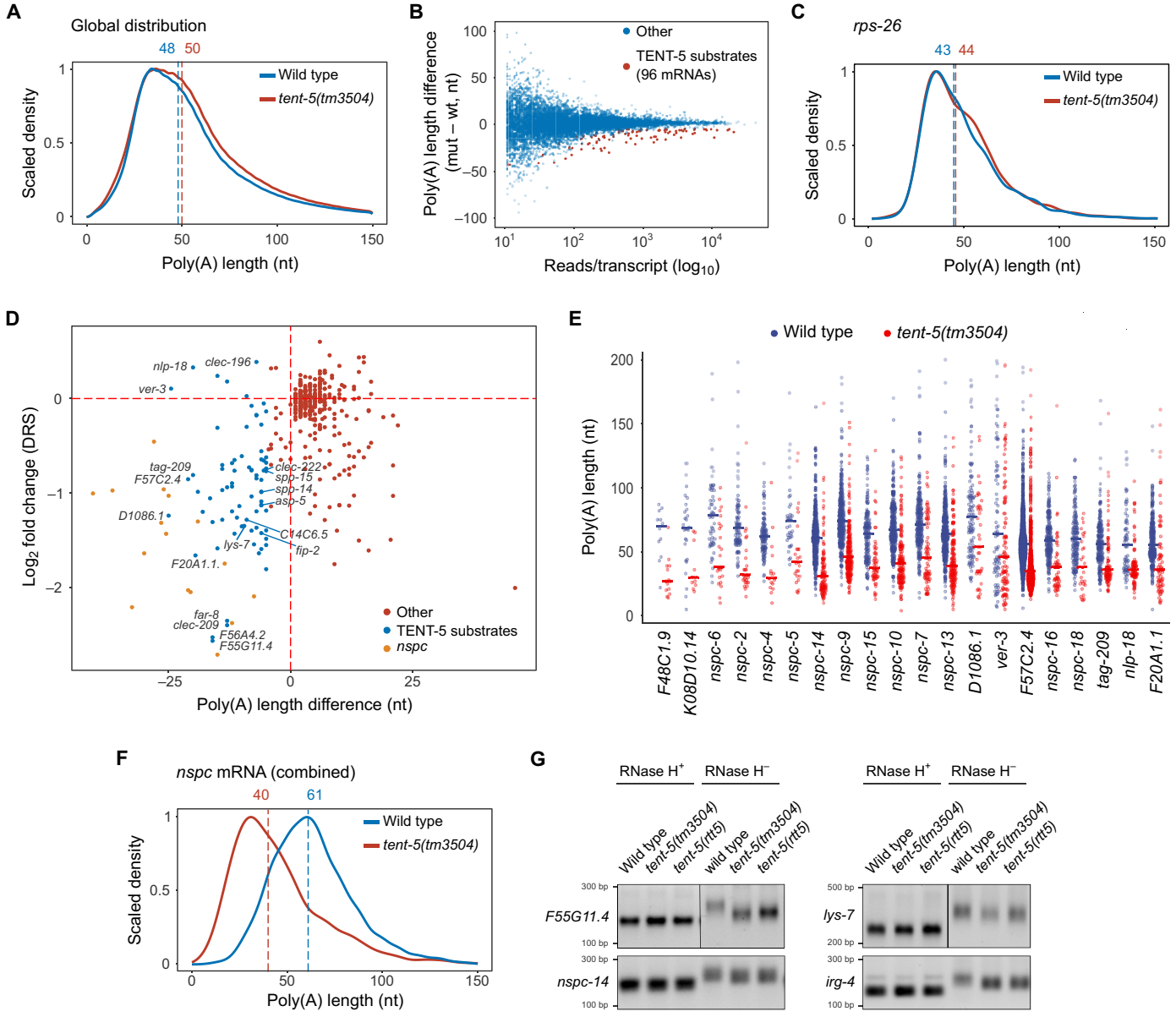

Fig. 5. Transcripts down-regulated in the *tent-5*–deficient mutants are the direct targets for polyadenylation by TENT-5. (**A**) DRS-based global poly(A) tail length profiling of mRNA isolated from *tent-5(tm3504)* and wild type. Density distribution plots are shown for all identified transcripts, scaled to 1. Vertical dashed lines represent median poly(A) lengths (in nucleotides) for each condition. (**B**) Plot showing expression levels and difference in the median poly(A) tail length between *tent-5* mutant and wild-type worms. TENT-5–regulated transcripts ($n = 96$) are indicated in red (FDR < 0.05). (**C**) *rps-26* mRNA that encodes ribosomal protein shows no change in the median poly(A) tail length between mutant and wild-type animals. Plot description as in (A). (**D**) The relationship between the median poly(A) tail length and the expression levels of respective mRNAs in *tent-5*–defective worms. Blue and orange dots indicate TENT-5 substrate mRNAs ($n = 96$). For readability, only IDs of the top 20 substrates and mentioned immune effectors are indicated. (**E**) Bee swarm plots of poly(A) tail length distributions for the top 20 TENT-5 molecular substrates ordered by the median poly(A) tail length fold change. Horizontal lines indicate the median poly(A) tail length for each transcript. (**F**) mRNAs that encode NSPC proteins show significant shortening of the median poly(A) tail length in mutant worms. Plot description as in (A). (**G**) Poly(A) tail PCR tests (PAT) of selected TENT-5–regulated transcripts. Before sample preparation for PAT, samples were treated with RNase H in the presence of oligo(dT)$_{25}$ (RNase H$^+$). PCR products were analyzed on 2% agarose gels.

and the level of respective mRNAs in *tent-5*–defective worms and observed that transcripts with shorter poly(A) tails exhibited a significant decrease in their levels, including for multiple members of the *nspc* gene family (Fig. 5D). The observed correlation between the poly(A) tail length and mRNA level strongly suggests that polyadenylation by TENT-5 increases the stability of target transcripts.

Next, we addressed the impact of polyadenylation by TENT-5 on mRNAs that encode innate immune effectors. We observed that the median poly(A) tail length of mRNAs that encode proteins that contain CUB domains (e.g., *F55G11.4*), CLECs (e.g., *F56A4.2* and *clec-196*), lysozymes (e.g., *lys-7*), and other proteins involved in host defense (e.g., *F48C1.9*, *C14C6.5*, *asp-12*, and *spp-14*) were significantly decreased in the *tent-5(tm3504)* mutant (fig. S5H). We also noticed that 11 mRNAs that encode collagens had 5- to 9-nt shorter median poly(A) tails length in mutant worms (fig. S5I), suggesting that, similarly to mouse *Tent5a* KO (*26*), deficiency of *tent-5* in worms may cause some defects in an extracellular matrix (ECM) formation. Regulation of collagen genes and ECM has been shown to affect a worm's defense (*55*–*58*). Notably, at the top of the list of transcripts with the most significantly shortened poly(A) tails in mutant worms (Fig. 5E and data S4) were *nspc* genes, referred to above. The median poly(A) tail length of all *nspc* mRNAs was decreased from 61 to 40 nt in *tent-5(tm3504)* worms (Fig. 5F). As mentioned above, we also identified *nspc* among genes whose expression levels were most significantly down-regulated in *tent-5*–deficient worms, both by RNA-seq (fig. S5J and data S1) and DRS (Fig. 5D and data S5). Genes from the *nspc* family are rapidly evolving and encode 18 almost identical short (~100 amino acids) proteins that have been proposed to encode antimicrobial peptides (*33*). Next, we examined the poly(A) tail length of four representative transcripts, including *nspc-14*, using poly(A) PCR tests (PAT) that revealed that amplicons from both *tent-5*–deficient mutants were shorter compared to those from wild-type worms (Fig. 5G and fig. S5K). Digestion with ribonuclease H (RNase H) proved that the observed differences resulted from the change in the poly(A) tail length (Fig. 5G). Together, our results lead us to propose that TENT-5 has a stabilizing effect on a specific subset of mRNAs by extending their poly(A) tails.

TENT-5 regulates mRNAs that encode secreted proteins

To determine what distinguishes TENT-5 ncPAP substrates from other mRNAs, we performed a comprehensive analysis of their sequences. First, we observed that TENT-5 substrate mRNAs were shorter (Fig. 6, A and B) and had shorter 3′UTRs (Fig. 6C) compared to all other transcripts identified by DRS. At the same time, there was no difference in 5′UTR length between the TENT-5–regulated and nonregulated mRNAs (fig. S6A). We observed similar effects for the mRNAs of genes whose expression levels were down-regulated in *tent-5(tm3504)* mutant worms compared to wild type according to RNA-seq (fig. S6, B to E). Next, we sought to find linear sequence motifs that were specifically enriched in coding or 3′UTR sequences of mRNAs, whose poly(A) tails were shorter in *tent-5*–deficient worms. We found no specific motifs across these transcripts, although note that the DREME (Discriminative Regular Expression Motif Elicitation) motif discovery tool (*59*) we used only enables the identification of relatively short motifs (up to 8 nt).

However, we noticed that many of the genes for which expression was significantly down-regulated in mutant worms were annotated as encoding proteins of the extracellular space (Fig. 2B and fig. S5C). In *C. elegans*, roughly 19% of all proteins are predicted to have an N-terminal signal peptide that targets them toward the secretory pathway through the endoplasmic reticulum (ER) (*60*). Notably, we observed that as much as 71 and 80% of genes down-regulated in *tent-5*–deficient worms at least 1.5-fold (RNA-seq and DRS, respectively) and 84% of all TENT-5 substrates (DRS) encoded proteins with a predicted signal peptide (Fig. 6D, fig. S6F, and data S4), strongly indicating that TENT-5 is responsible for the polyadenylation of mRNAs that encode ER-targeted secreted proteins. Transcripts that encode secreted antimicrobial proteins, such as lysozymes, caenopores (SPP), and proteins containing CLEC or CUB domains, and some enzymes involved in extracellular macromolecule digestion were remarkably overrepresented among the genes that were down-regulated in *tent-5(tm3504)* mutants (Fig. 3D and fig. S3E) and carried shorter poly(A) tails (fig. S5H). As we observed such a prominent enrichment of mRNAs that encode secreted proteins among TENT-5 substrates and as in worms, the expression of roughly one-third of all genes encoding secreted proteins are induced during infection (*31*, *60*); this could explain the higher susceptibility of *tent-5* mutant to the infection.

Given that TENT-5 regulates levels of mRNAs that encode secreted proteins, we aimed to test whether it is enriched at the ER in the intestinal cells, which have large rough ER (*61*). Although adult *C. elegans* intestines are known to contain multiple autofluorescent gut granules (*62*), we confirmed that granules observed in the *tent-5 (rtt6[tent-5::gfp::3xflag] I)* knockin strain (Fig. 1F) do not result from the aggregation of TENT-5-GFP. The chromatography analysis of total protein extracts from the *tent-5(rtt6)* worms revealed that most of the protein is present in the fraction corresponding to the TENT-5-GFP molecular weight (fig. S6G). However, a small amount of TENT-5 was also found in macromolecular complexes or aggregates. The expression levels of TENT-5 (fig. S1E) and animal viability (fig. S6H) of *tent-5::gfp* strain were unaltered in comparison to the wild-type animals, pointing to the expression of functional protein. Nevertheless, to avoid the misinterpretation of the microscopic results due to the possible presence of aggregates, we excluded the strongest signals observed in a GFP channel from the subsequent colocalization analysis. To test whether TENT-5 localizes to the ER, we crossed *tent-5::gfp* worms (Fig. 1F and fig. S1, E to H) with a transgenic strain expressing the ER marker protein TRAM-1 (translocating chain-associating membrane protein transporter) fused to a CemOrange2 fluorescent protein designed to be exclusively expressed in the intestine (*vkEx2664 [nhx-2p::CemOrange2::tram-1, myo-2p::gfp]*) (*63*). The microscopic analysis revealed partial colocalization of CemOrange2–TRAM-1 and TENT-5–GFP (Pearson correlation coefficient: 0.4 ± 0.11 SD, $n = 18$) (Fig. 6E), indicating that a fraction of TENT-5 localizes to the ER. This observation is in agreement with the recently published data showing that TENT5C partially localizes to ER in mammalian cells (*23*, *64*, *65*). To analyze TENT-5 association with ER further, we performed a subcellular protein fractionation of whole worm extracts prepared from wild-type, *tent-5::gfp*, and *vgln-1::mKate2 (vgln-1(rtt9[vgln-1::mKate2:::3xmyc] II)* strains. VGLN-1 (ViGiLN homolog) is localized in the cytoplasm and nucleus (*66*), and its human ortholog, HDLBP (high density lipoprotein binding protein), has been also shown to be associated with the ER (*67*). Subcellular protein fractionation confirmed that TENT-5–GFP resides in the cytosol but is also present at membranes, including ER (Fig. 6F and fig. S6, I and J). Our results allow speculating that TENT-5 might be targeted to at least some of its substrates by colocalization with ER-translated short mRNAs. However, the exact mechanism of the TENT-5 substrate specificity remains to be elucidated.

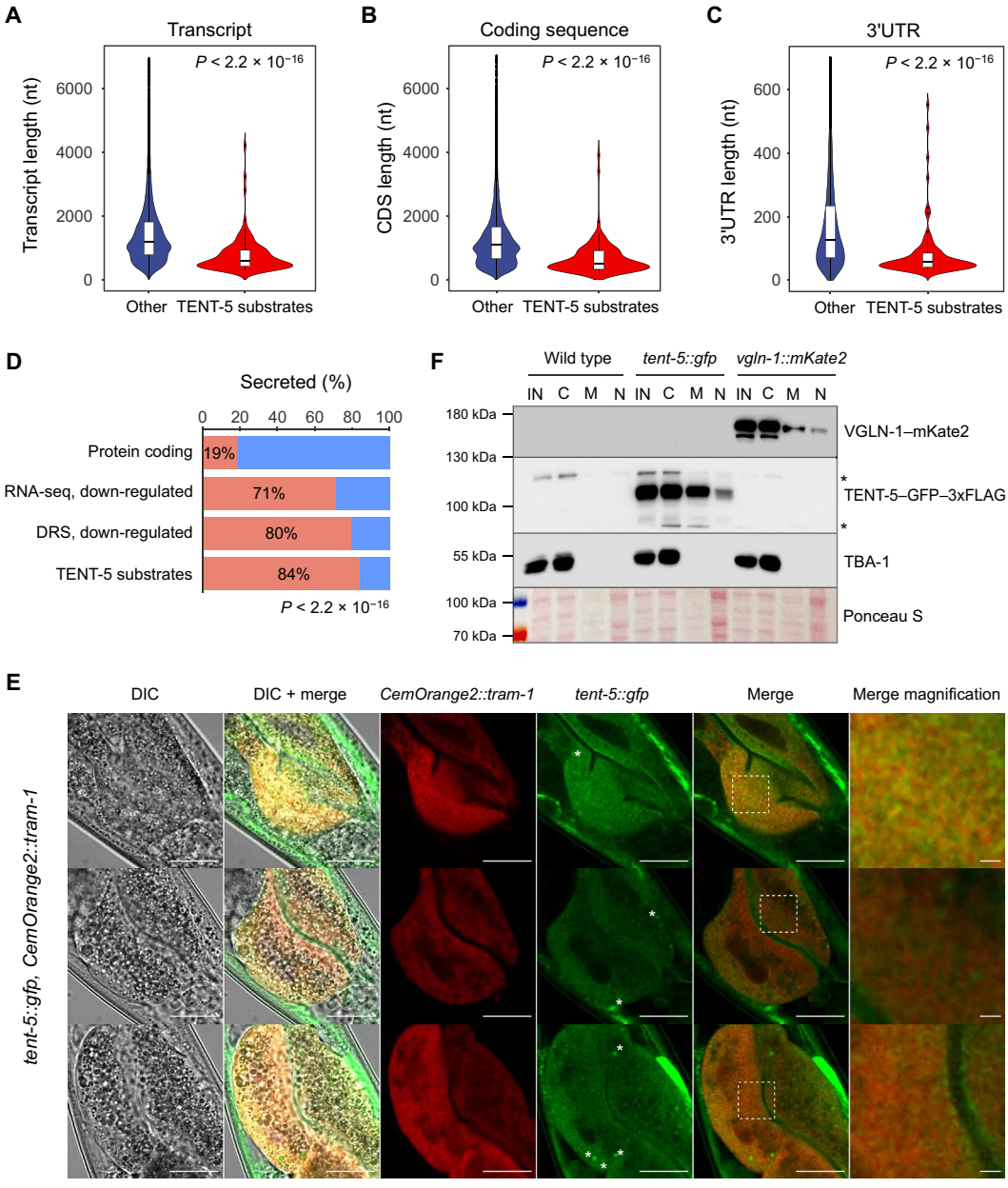

Fig. 6. TENT-5 regulates mRNAs that encode secreted proteins. Violin plots showing length distribution of transcripts (**A**), coding sequence (**B**), and 3′UTRs (**C**) of TENT-5 substrates ($n = 96$) compared to other transcripts identified by DRS ($n = 16{,}568$) (*P* value, Wilcoxon test). (**D**) Fractions of genes that encode secreted proteins (red) as defined in (*60*) across indicated datasets: expressed protein-coding genes (WS270; RNA-seq, base mean > 0), RNA-seq and DRS *tent-5(tm3504)* down-regulated genes [FDR < 0.05, $\log_2$FC < –log2(1.5)], and TENT-5 substrates. *P* value for enrichment of genes encoding secreted proteins in each group versus whole genome is $<2.2 \times 10^{-16}$ (Fisher's exact test). (**E**) Representative fluorescence and DIC microscopy images of distal parts of the adult worms' intestines, which coexpress TENT-5-GFP and ER marker protein CemOrange2–TRAM-1. Both tagged proteins partially colocalize at the ER (Pearson correlation coefficient: 0.4 ± 0.11 SD, 18 worms). Analysis was restricted to cells expressing CemOrange2–TRAM-1, and the strongest unspecific signal from the green channel (examples are marked with asterisks) was excluded from the analysis. White dashed squares in the merge picture indicate the region magnified on the right. Scale bars, 20 μm (all pictures) and 2 μm (magnification). (**F**) TENT5C is present in the ER fraction. Subcellular fractionation of proteins isolated from wild-type, *tent-5::gfp::3xflag*, and *vgln-1::mKate2:::3xmyc* strains followed by Western blot. Anti-tubulin (TBA-1) and anti–red fluorescent protein (VGLN-1–mKate2) antibodies and Ponceau S staining were used as fractionation controls. IN, input; fractions: C, cytoplasmic; M, membrane; N, nuclear. Asterisks indicate nonspecific bands.

The role of TENT-5 in innate immunity is evolutionarily conserved

Because TENT-5 is orthologous to mammalian TENT5 ncPAPs, we hypothesized that mammalian TENT5 proteins might also have a role in innate immunity. Murine macrophages, key innate immune effector cells, express two of the four *Tent5* genes, *Tent5a* and *Tent5c*. We found that both genes were induced in bone marrow–derived macrophages (BMDMs) upon stimulation with lipopolysaccharide (LPS), which is a potent activator of inflammatory and immune response in M1 macrophages (Fig. 7A) (*68*). To test whether TENT5A

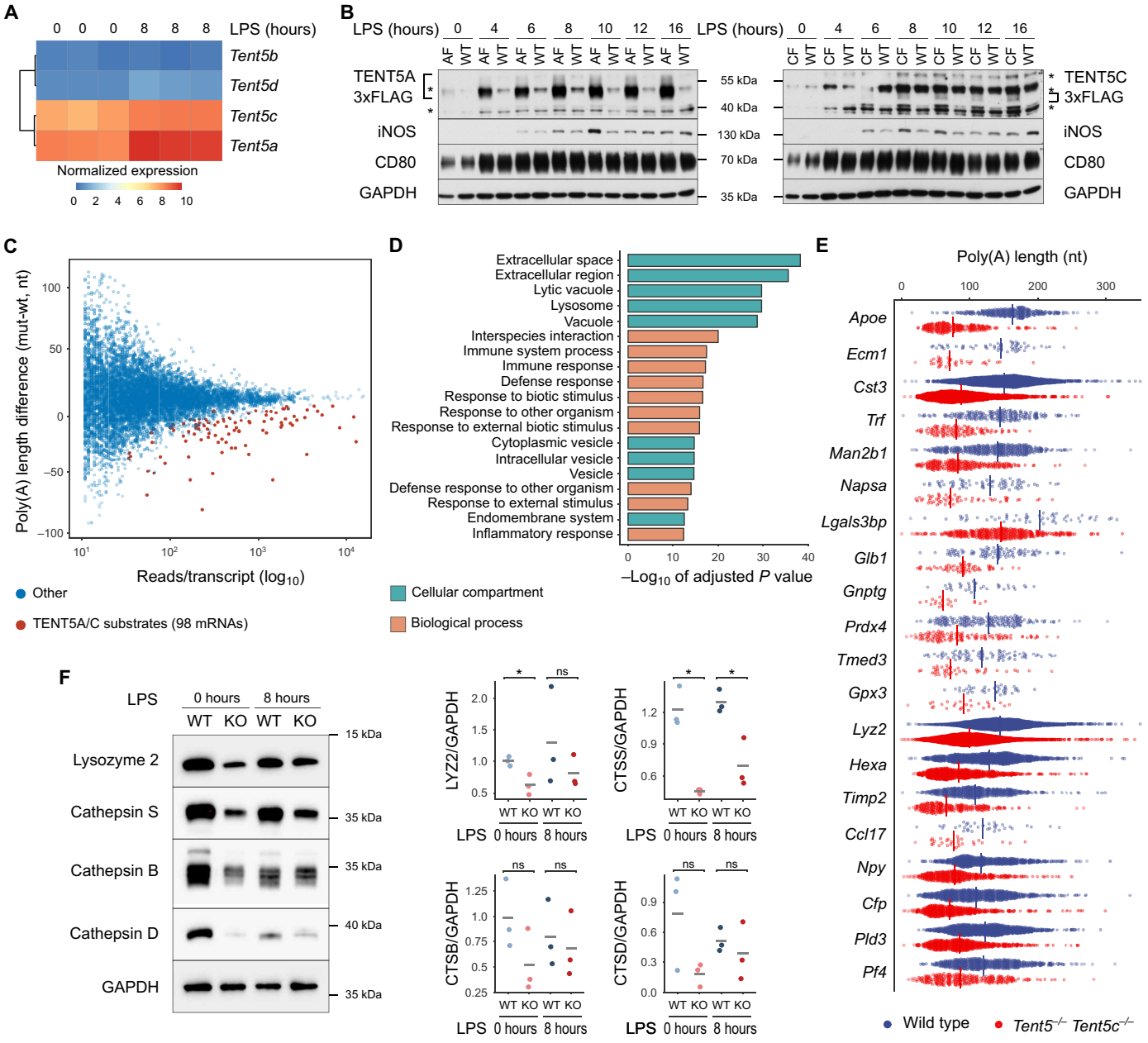

Fig. 7. The role of TENT-5 in innate immunity is evolutionarily conserved. (**A**) Heatmap showing expression levels of *Tent5* genes in BMDMs isolated from the wild-type mice. Stimulation of BMDMs with LPS led to increased expression levels of *Tent5a/c*. (**B**) TENT5A/C were elevated in macrophages stimulated with LPS as illustrated by anti-FLAG immunoblots on extracts prepared from wild-type (WT), TENT5A-3xFLAG (AF), and TENT5C-3xFLAG (CF) BMDMs. iNOS and CD80 levels serve as a control of BMDM activation. The lines and asterisks indicate specific and unspecific bands, respectively. (**C**) Plot showing expression levels and difference in the median poly(A) tail length of mRNAs that were isolated from *Tent5a*$^{-/-}$ *Tent5c*$^{-/-}$ and wild-type BMDMs. TENT5A/C-regulated transcripts ($n = 98$) are marked in red (FDR < 0.05). (**D**) Top 20 (ordered by adjusted *P* value) GO terms of TENT5A/C substrate mRNAs (data S6). (**E**) Bee swarm plots of poly(A) tail length distributions for the top 20 TENT5A/C molecular substrates ordered by the median poly(A) tail length fold change (data S6). (**F**) Western blots showing that the lack of TENT5A/C leads to the lower abundance of indicated peptides both in unstimulated (LPS; 0 hours) and stimulated (LPS; 8 hours) BMDMs. Glyceraldehyde phosphate dehydrogenase (GAPDH) serves as a loading control. Shown is the representative result of three biological replicates (fig. S7K). Graphs on the right show values of the band intensity ratio between tested protein and GAPDH. Points indicate values of each of three biological replicates, and lines denote the average value for biological replicas. *$P \leq 0.05$ (two-tailed *t* test).

and TENT5C proteins also were activated during infection, we examined their levels in the time course of LPS treatment in BMDM isolated from TENT5A-3xFLAG (*26*) and TENT5C-3xFLAG knockin mouse lines (*21*). The effectiveness of BMDM activation was examined by analysis of M1 macrophage polarization markers inducible nitric oxide synthase (iNOS) and CD80 (Fig. 7B) (*69*). Similarly, TENT5A-3xFLAG and TENT5C-3xFLAG levels were elevated in response to LPS stimulation (Fig. 7B), consistent with the notion that the role of TENT5 ncPAPs in innate immunity could be evolutionarily conserved.

To determine the physiological relevance of TENT5A and TENT5C in macrophages, we aimed to analyze the phenotypes of mice devoid of *Tent5a* and *Tent5c* genes. *Tent5c* KO mice do not exhibit any gross phenotypes (*21*, *23*, *70*), whereas *Tent5a* KO are smaller than wild type and display skeletal abnormalities (*26*). The double KO of *Tent5a* and *Tent5c* leads to preweaning lethality that suggests potential redundancy between two ncPAPs. To overcome the lethality of the double *Tent5a Tent5c* KO, we used the *Tent5a*$^{Flox/Flox}$ *Tent5c*$^{-/-}$ mouse line that was obtained by crossing *Tent5a*$^{Flox/Flox}$ conditional KO (cKO) with the previously described *Tent5c*$^{-/-}$ KO line (*21*). We have isolated BMDMs from *Tent5a*$^{Flox/Flox}$ *Tent5c*$^{-/-}$ and wild-type mice and delivered Cre recombinase to macrophages by lentiviral transduction that allowed us to obtain vital *Tent5a*$^{-/-}$ *Tent5c*$^{-/-}$ cells. Next, we treated BMDMs with LPS for 8 hours, a time point when expression of TENT5A and TENT5C is highly elevated (Fig. 7, A and B), and collected cells for subsequent analyses. To identify potential TENT5A and TENT5C substrates in activated macrophages, we performed transcriptome-wide poly(A) tail profiling by DRS. We obtained approximately 8 million transcriptome-wide reads from two *Tent5a*$^{-/-}$ *Tent5c*$^{-/-}$ and two wild-type samples (data S6). Again, the global distribution of the median poly(A) lengths was consistent with previous reports (*52*). We observed no differences in the global polyadenylation status between *Tent5a*$^{-/-}$ *Tent5c*$^{-/-}$ and wild-type samples (fig. S7A), as well as changes in the median poly(A) tail length of mRNAs encoding ribosomal proteins (fig. S7B). We found that in BMDMs isolated from *Tent5a*$^{-/-}$ *Tent5c*$^{-/-}$ BMDMs, 98 mRNAs had median poly(A) tail lengths shorter (FDR < 0.05) in comparison to the samples obtained from the wild type (Fig. 7C and data S6). Many of these mRNAs were also identified as molecular substrates for TENT5A or TENT5C in osteoblasts (*26*) and multiple myeloma cell lines (fig. S7C) (*21*), indicating that they represent direct substrates for polyadenylation by TENT5A/C. GO analysis of TENT5A/C substrate mRNAs revealed their strong association with the extracellular space, defense and innate immune response, and lytic vacuole (Fig. 7D and data S6), recapitulating observations obtained with *tent-5* mutant worms. Notably, only 14 mRNAs had median poly(A) tail length at least 5 nt longer in *Tent5a*$^{-/-}$ *Tent5c*$^{-/-}$ cells compared to wild type (data S6). Some of these mRNAs also show an association with immune response and extracellular space (data S6) that, similar to our observations in worms, may indicate compensatory effects in cells with defective immune responses. We did not attempt to establish the relationship between the poly(A) tail length and the expression levels of the respective mRNAs, as only one gene (*Lgals3bp*) was differentially expressed between *Tent5a*$^{-/-}$ *Tent5c*$^{-/-}$ and wild-type samples (data S6).

In line with our observations in worms, a comprehensive analysis of TENT5A/C-regulated transcripts revealed that they were shorter (fig. S7, G and H), tended to have shorter 3′UTRs (fig. S7I), and tended to have moderately shorter 5′UTRs (fig. S7J) compared to other transcripts detected in macrophages by DRS. Analysis of TENT5A/C substrates identified no sequence motif enrichment across their 3′UTRs. Fifty-nine of 98 (~60%) TENT5A/C substrate mRNAs encode extracellular space proteins (data S6), suggesting that TENT5A/C preferentially polyadenylates mRNAs that encode secreted proteins, many of which (32 of 59) have a role in the immune response. Among mRNAs with shorter median poly(A) tail length in *Tent5a*$^{-/-}$ *Tent5c*$^{-/-}$ macrophages (Fig. 7E and data S6) were mRNAs that encode lysozyme (*Lyz2*) (fig. S7D) and lysosomal proteases cathepsins (*Ctsd* and *Ctsb*) (fig. S7, E and F). These proteins transit the ER during their maturation and are homologous to TENT-5 substrates in worms, and their role in the mammalian immune response is well documented (*71*–*77*). Therefore, we examined whether the lack of TENT5A and TENT5C affects the protein levels of lysozyme and cathepsins. We have observed a definite but modest drop in LYZ2 and cathepsins (Fig. 7F and fig. S7K) levels in *Tent5a*$^{-/-}$ *Tent5c*$^{-/-}$ BMDMs, confirming the direct effect of cytoplasmic polyadenylation by TENT5A/C on innate immunity-related protein expression. Our observation that in BMDM devoid of *Tent5a* and *Tent5c*, the shortening of the poly(A) tails of a specific group of mRNAs is not accompanied by significant down-regulation of these mRNAs' expression but affects levels of respective proteins allows speculating that at least in activated BMDM, cytoplasmic polyadenylation may have a more prominent influence on translation efficiency than on mRNA stability. On the basis of our results, we concluded that the enzymatic activity of TENT5A/C plays a role in the physiology of murine macrophages and, similarly to its ortholog in worms, may facilitate the innate immune response.

DISCUSSION

In its natural habitat, *C. elegans* encounters numerous and diverse pathogens. Worms' fitness and rapid adaptation to an ever-changing microbial environment require dynamic and highly efficient modulation of the immune response. It is widely appreciated that in animals, innate immunity is orchestrated by a plethora of transcriptional and posttranscriptional mechanisms (*7*, *78*–*80*). The posttranscriptional aspect of innate immune regulation in worms is a fast-growing field of research (*58*, *81*–*84*). *C. elegans* can sense bacterial noncoding RNAs to induce avoidance of a pathogen (*85*). A few reports have also implicated microRNAs in host defense (*86*–*88*), whereas viral RNA uridylation, by one member of the TENT family, CDE-1, has been shown to play a role in the antiviral response (*89*). Cytoplasmic polyadenylation is a powerful posttranscriptional mechanism that shapes the transcriptome and consequently also the proteome, through the regulation of mRNA stability and translation efficiency. This work shows that cytoplasmic polyadenylation by ncPAP TENT-5 positively regulates innate immunity in *C. elegans*.

TENT-5 is a cytoplasmic protein that is expressed through the whole life cycle of the worm in multiple cells of the body, including the intestine (Fig. 1). In worms, the immune response and digestion are connected. Many enzymes responsible for the macromolecular degradation of food participate in the degradation of pathogen-derived macromolecules (*61*). Upon infection with bacterial pathogens that infect through the gut, intestinal cells secrete a large amount of enzymes and antibacterial proteins. Intestinal cells must have an enormous capacity for protein synthesis and secretion. Our results show that TENT-5 preferentially polyadenylates and stabilizes mRNAs that encode short secreted proteins with a role in digestion and immunity (Figs. 5 and 6). The length of the poly(A) tail is critical for mRNA stability, and the posttranscriptional lengthening of mRNAs' poly(A) tails in the cytoplasm may thus extend their half-life. Such a mechanism, extending mRNA longevity and promoting translation, would be not only energy effective but also extremely fast, a valuable feature when a rapid reaction to changing environmental conditions is needed, for example, during immune or stress responses.

The relevance of TENT-5 in innate immunity is also supported by the reduced survival of *tent-5*–deficient worms upon infection with a range of bacterial pathogens (Fig. 4). Mutant worms display

a moderately reduced life span also when grown on *E. coli*. Furthermore, this survival defect is associated with the increased bacterial load in the intestine of the *tent-5*–deficient worms. This observation may suggest that because of the decreased basal expression of genes encoding digestive enzymes and cytoprotective proteins, mutant worms have limited ability to deal even with relatively nonpathogenic food, exhibiting reduced life span. In such an interpretation, TENT-5 may not be solely dedicated to innate immunity but rather influence stability and potentially translation efficiency of many mRNAs encoding secreted proteins. The consequences of *tent-5* deficiency are, however, most evident under physiological conditions when secretion plays a life-saving role. The fact that TENT-5 is up-regulated upon infection may be explained by specific pathogen–induced transcriptional regulation or by a mechanism that senses the demand for efficient protein secretion. Further research will be needed to determine what other secretion-dependent processes are regulated by TENT-5.

Direct sequencing of RNA samples prepared from *tent-5* mutants and wild-type worms allowed us to uncover substrates of TENT-5 enzymatic activity (Fig. 5). Our analysis of poly(A) tails lengths in L4 *C. elegans* is consistent with previous results (*52*, *53*). Those studies identified a negative correlation of poly(A) tail length with mRNA expression. Given the counterintuitive nature of these observations, we sought to take advantage of the high quality of our DRS data and analyzed the relationship between these features. In accordance with (*52*, *53*), our data showed a similar phenomenon (fig. S5). However, TENT-5 substrate mRNAs showed significantly decreased expression levels in *tent-5(tm3504)* mutants, suggesting that shortening of the poly(A) tail from its wild-type length lowers mRNAs expression (Fig. 5). Thus, our results show that for TENT-5 substrates, an increase in poly(A) tail length sustains mRNA steady-state levels.

Our data indicate that TENT-5 affects mRNAs that encode short secreted proteins. Among the prominent TENT-5 targets are mRNAs of the *nspc* family of genes for which mRNA polyadenylation and expression are strongly decreased in the *tent-5* mutant (Fig. 5). In our previous studies, we also found that TENT5 family members regulate the expression of genes encoding secreted proteins. In B cells, TENT5C polyadenylates mRNAs that encode immunoglobulins (*23*), and in osteoblasts, the main substrates of TENT5A are mRNAs encoding collagens (*26*). In line with that, we show that mRNAs that encode secreted proteins constitute a large fraction of TENT5A and TENT5C direct substrates in macrophages (Fig. 7). In agreement with the nature of TENT5 substrates, these poly(A) polymerases are associated with the ER, and this is probably the main determinant of their substrate specificity. It was recently shown that TENT5C is actively recruited to ER in human cells through interaction with fibronectin type III domain–containing proteins FND3CA and FNDC3B (*64*, *65*). Disturbance of TENT5C function leads to ER shrinking, destabilization of ER-translated mRNAs, and defects in ER-mediated protein folding and secretion (*64*). It is probable that TENT5C's binding to the ER, mediated by FNDC3A and FNDC3B, may be enough to target its substrates. Whether the worm's TENT-5 target selection corresponds to an analogous mechanism requires further investigation, because among proteins with fibronectin type III domains, there are no obvious FNDC3 orthologs encoded in the genome. Controlling the secretory capacity of the ER is key for resistance to infection (*90*, *91*). Cytoplasmic polyadenylation by TENT5 proteins of mRNAs encoding proteins that transit the ER provides a new layer to the regulation of secretion essential for the proper immune response and other physiological processes such as bone formation in vertebrates.

Last, we demonstrate that the role of TENT-5 in innate immunity is evolutionarily conserved. In murine macrophages, TENT-5 orthologs, TENT5A and TENT5C, polyadenylate mRNAs that encode lysozyme and cathepsin proteases (Fig. 7), increasing their protein level. Lysozyme is one of the most abundant antimicrobial proteins secreted by macrophages, and deletion of *Lyz2* increases susceptibility to infection with *P. aeruginosa*, *Micrococcus luteus*, and *Klebsiella pneumoniae* due to impaired clearance of pathogen and can lead to higher host mortality (*71*–*74*). Cathepsins not only play a notable role in lysosomal protein breakdown but also regulate the immune response (*92*). BMDMs isolated from *Ctsd*-deficient mice display enhanced susceptibility to *Listeria monocytogenes* infection and increased intraphagosomal viability of bacteria (*75*). Moreover, cathepsin D protein levels were up-regulated after infection of murine macrophages with *Bacillus subtilis*, *P. aeruginosa*, *L. monocytogenes*, *S. aureus*, and *E. coli*, and again, its deficiency led to an increase in the amounts of each of these bacteria inside populations of macrophages (*76*). Cathepsin B was also required for optimal posttranslational processing of tumor necrosis factor–α (TNF-α) in response to LPS, and BMDMs from *Ctsb*-deficient mice secrete significantly less TNF-α than wild-type macrophages (*77*).

Our work demonstrates the conserved role of mRNA polyadenylation and TENT5 family ncPAPs in the regulation of innate immunity in animals. Taking into account that, in worms, TENT-5 is expressed in multiple tissues, we expect that its functions go beyond protection against pathogens and may be generally important for physiological processes that involve protein secretion. In mammals, TENT5A to TENT5D are expressed in different tissues and developmental stages, opening the possibility for them to have broad biological significance and functional interactions too.

MATERIALS AND METHODS

Bacterial strains and culture

E. coli HB101 was cultured at 37°C in LB medium supplemented with streptomycin (final concentration of 0.1 mg/ml). *P. aeruginosa* PAO1 and *S. marcescens* Db10 were grown at 37°C in LB medium without antibiotics (*48*, *93*). *P. luminescens* Hb was grown at 30°C in LB medium without antibiotics (*48*). *S. aureus* NCTC 8325 (Argenta Ltd.) was cultured at 37°C on tryptic soy agar (TSA) or tryptic soy broth (TSB) (both from BD Biosciences) supplemented with nalidixic acid (Nal) (final concentration of 10 μg/ml). *E. coli* DH5α and MH1 strains were cultured at 37°C in LB supplemented with appropriate antibiotics. All antibiotics were purchased from Sigma-Aldrich.

C. elegans strains and maintenance

C. elegans was maintained on nematode growth medium (NGM) plates seeded with *E. coli* HB101 at 20°C unless otherwise specified. Strains obtained from the National Bioresource Project of Japan (NBRP) and strains generated by the CRISPR-Cas9 were outcrossed two to nine times to the wild-type strain. The following *C. elegans* strains were used: N2 Bristol (wild type) and VK2664 (*vkEx2664 [nhx-2p::CemOrange2::tram-1, myo-2p::gfp]*) strains were obtained from the Caenorhabditis Genetics Center; *tent-5(tm3504) I* was obtained from NBRP; ADZ20 (*tent-5(rtt5) I*), ADZ21 (*tent-5(rtt6[tent-5::gfp::3xflag]) I*), and ADZ24 (*vgln-1(rtt9[vgln-1::mKate2:::3xmyc] II*) were generated in this study; ADZ87 (*tent-5(rtt6[tent-5::gfp::3xflag])*

I, vkEx2664 [nhx-2p::CemOrange2::tram-1, myo-2p::gfp]) strain was obtained by crossing ADZ21 with VK2664.

C. elegans transgenic strain generation

Transgenic worm strains were generated using standard microinjection protocols. Plasmids that were used for microinjections were purified with PureLink mini-prep kit (Thermo Fisher Scientific, K210002). Injections were conducted using the Axio Observer D1 inverted microscope (Zeiss) equipped with a Femto Jet 4i microinjection system (Eppendorf). For each transformation, at least two independent transgenic strains were obtained. All oligonucleotides and DNA constructs used for transgenic strain generation are listed in tables S2 and S3, respectively.

The KO strain ADZ20 *tent-5(rtt5) I* that harbors a 2909–base pair deletion, which spans from the start to stop codon of *tent-5* isoform d, was generated using an adapted version of the CRISPR-Cas9 protocol (*94*). Mutation in the *dpy-10* gene was used as a CRISPR co-conversion marker. Single-stranded DNA (ssDNA) encoding tracrRNA (trans-activating CRISPR RNA) and CRISPR RNA (crRNA) with 20 N of single-guide RNA (sgRNA) sequences was used for the preparation of templates for in vitro sgRNA synthesis. Briefly, 5 µl of 100 µM VL311 tracrRNA oligo was annealed with 5 µl of 100 µM sgRNA oligo (VL312, VL313, and VL315) in the 50-µl mix containing deoxynucleotide triphosphates, Phusion buffer, and Phusion Hot Start II Polymerase and incubated at 98°C for 3 min; 98°C for 10 s, 65°C for 20 s, and 72°C for 5 s for 10 cycles; and 72°C for 5 min. The reaction was purified with AMPure XP magnetic beads [1:1.4 (v/v) mix to beads; Beckman Coulter, A63882]. In vitro transcription was assembled by mixing 400 ng of DNA template in 35 µl of RNase-free water, 5 µl of ribonucleoside triphosphates (NTPs) mix (20 mM each), 10× transcription buffer [200 mM tris-HCl (pH 7.9), 30 mM $MgCl_2$, 50 mM dithiothreitol (DTT), 50 mM NaCl, and 10 mM spermidine], 1.25 µl of RiboLock RNase Inhibitor (40 U/µl) (Thermo Fisher Scientific, EO0384), and 4 µl of T7 polymerase (homemade). Eight reactions were set up for the single sgRNA transcription. Following incubation at 37°C for 3 hours, each sample was treated with 0.5 µl of TURBO deoxyribonuclease (DNase) (2 U/µl; Thermo Fisher Scientific, AM2239) at 37°C for 30 min. RNA was purified from the pooled reactions with the phenol/chloroform extraction and purified further through electrophoresis in 6% urea polyacrylamide gel electrophoresis (PAGE). Animals were injected with the following mix: 15.5 µM Cas9 (Cas9::NLS_{SV40}::His_6 protein; homemade), 5.9 µM sgRNA–dpy-10, 11 µM sgRNA–tent-5-1, 11 µM sgRNA–tent-5-2, 0.44 µM single-stranded oligodeoxynucleotide (ssODN)–dpy-10, 0.88 µM ssODN–tent-5, 150 mM KCl, and 20 mM Hepes (pH 8.0). Worms showing dumpy phenotype in F_1 progeny were screened for *tent-5* deletion using PCR, and, later, the deletion was confirmed by Sanger sequencing. Mutant worms were backcrossed two times to wild-type worms to cross out the *dpy-10* mutation and CRISPR off-targets.

The knockin strain ADZ21 *tent-5(rtt6[tent-5::gfp::3xflag]) I* was generated by CRISPR-Cas9 according to (*95*). The gRNA sequence (5′-TGCCACCAGATGCAGCTACA-3′) was cloned into pDD162 to generate pDD162_*sgRNA425*. Homology arm regions were amplified by PCR using genomic DNA (gDNA) as a template and were inserted into pDD282, resulting in the pDD282-*tent-5::gfp::3xflag* construct. N2 worms were injected with the following mix: pDD282-*tent-5::gfp::3xflag* (10 ng/µl), pDD162_*sgRNA425* (50 ng/µl), *myo-2p::mCherry* pharyngeal coinjection marker pCFJ90 (2.5 ng/µl), and *myo-3p::mCherry* body wall muscle coinjection marker pCFJ104 (5 ng/µl). The selection of positive knockin candidates was performed as described (*95*). Animals with successful GFP-tag insertion were backcrossed three times with the wild-type strain to get rid of CRISPR off-target effects. The knockin strain ADZ24 *vgln-1(rtt9[vgln-1::mKate2:::3xmyc] II* was generated by CRISPR-Cas9 using constructs encoding gRNA, pDD162_*sgRNA456* (gRNA sequence: 5′-CGTTCTTTACCAACGACGAG-3′), and homology arm regions, pDD287-*vgln-1::mKate2::3xmyc*.

Plasmid construction

General cloning techniques were conducted according to the well-established protocols (*96*) or manuals provided by the manufacturers of kits. All plasmids were generated using either classical restriction enzyme digestion and ligation or sequence- and ligation-independent cloning (SLIC) (*97*, *98*) and validated by digestion with restriction enzymes and sequencing. All oligonucleotides and DNA constructs are listed in tables S2 and S3. To generate pDD162-*sgRNA425* (pVL060), two PCRs were performed using pDD162 as a template, with primers VL342 and VL344 and with VL343 and VL345. Fragments were gel-purified and used in a 1:1 molar ratio as templates for PCR with primers VL386 and VL387. The product was purified from a gel and used for the SLIC with pDD162 that has been digested with Nde I and Sph I. pDD162-*sgRNA456* (pVL069) was cloned in a similar way using primers VL365 and VL364 instead of VL344 and VL345. pDD282-*tent-5::gfp::3xflag* (pVL062) was prepared as follows: Arms homologous to *tent-5* were amplified with VL347 and VL348 and with VL349 and VL350 on gDNA isolated from N2. pDD282 was digested with Avr II and Spe I, and the reaction was purified using a Clean-Up kit (A&A Biotechnology). For pDD287-*vgln-1::mKate2::3xmyc* construct (pVL070), homology arms were amplified from gDNA with primers VL366 and VL367 as well as VL368 and VL369. The pDD287 vector was digested with Avr II and Ngo MIV. In both cases, 200 ng of vector and 50 ng of each homology arm products were used for SLIC. The pClneo-NHA (N-terminal lambda symbolN boxB-binding domain and an HA-tag) constructs for tethering assays pCI-*NHA-tent-5*^{WT} and pCI-*NHA-tent-5*^{MUT} were cloned as follows: PCR products were generated with primers NHATENT-5_fw and NHATENT-5_rev on plasmids carrying *tent-5*^{WT} and *tent-5*$^{D151A, D153A}$ (isoform a) genes and subsequently cloned into Sal I and Not I sites of the pClneo-NHA.

Mice

All mice lines were generated by CRISPR-Cas9 in the Genome Engineering Unit (https://crisprmice.eu/) using methods described in (*21*, *23*, *26*). Briefly, a cKO *Tent5a*$^{Flox/Flox}$ (B6;CBA-*Tent5a*$^{Flox/Flox}$/Tar) mouse line was created by insertion of *LoxP* sites in introns flanking exon 2, which contains triplets encoding the catalytic center of the protein (D144N and D146N). Cas9-generated double-strand breaks in gDNA were targeted using two chimeric sgRNA. Bam HI restriction sites were inserted next to *LoxP* sites to facilitate genotyping. Donor mice were handled and injected as described before (*26*). The CRISPR cocktail consisted of mRNA Cas9 (25 ng/µl), sgRNAs (15 ng/µl), and ssDNA repair template (6 ng/µl). Correct integration of *LoxP* sites was confirmed by Sanger sequencing and followed by routine mice genotyping. Sequences of the sgRNAs, ssDNA donor, and primers used for sequencing and genotyping of *Tent5a*$^{Flox/Flox}$ mice can be found in table S2. Double *Tent5a*$^{Flox/Flox}$ *Tent5c*$^{-/-}$ mouse line was obtained by crossing *Tent5a*$^{Flox/Flox}$ cKO with the previously described *Tent5c*$^{-/-}$ (B6;CBA-*Tent5c*^{em1}/Tar) KO line (*21*). *Tent5c*-3xFLAG (B6;CBA-*Tent5c*$^{3xFLAG/3xFLAG}$/Tar) knockin mouse line

was generated as described in (*21*), with the exception that 3xFLAG was added instead of 1xFLAG. *Tent5a*-3xFLAG (B6;CBA-*Tent5a*$^{3xFLAG/3xFLAG}$) knockin line were described previously (*26*). Mice were bred in the animal house of Faculty of Biology, University of Warsaw and maintained under conventional conditions (*21*, *26*). All animal experiments were approved by the First Local Ethical Committee in Warsaw affiliated to the University of Warsaw, Faculty of Biology (approval numbers: WAW/176/2016 and WAW/772/2018) and were performed according to Polish Law (act number 266/15.01.2015) and in agreement with the corresponding European Union directive.

Primary BMDM cell culture

The primary BMDM cell cultures were established from the bone marrow monocytes isolated from *Tent5a*$^{Flox/Flox}$ *Tent5c*$^{-/-}$, *Tent5a*-3xFLAG, *Tent5c*-3xFLAG, and wild-type mice. Mice were euthanized by cervical dislocation at ages 13 to 22 weeks. Femurs and tibias were isolated, the ends of bones were cut, and the bone marrow was flushed with medium using a 25-gauge needle. Bone marrow cells were plated in Iscove's modified Dulbecco's medium (Thermo Fisher Scientific, 21980065) supplemented with 10% fetal bovine serum (FBS) (Gibco), penicillin (100 U/ml)/streptomycin (0.1 mg/ml) solution (Sigma-Aldrich), and macrophage colony-stimulating factor (10 ng/ml; PeproTech, 315-02) and cultured at 37°C in 5% CO_2 as described previously (*99*). For conditional gene targeting, BMDMs derived from *Tent5a*$^{Flox/Flox}$ *Tent5c*$^{-/-}$ and wild-type mice were transduced on the 8th day after isolation with 1 ml of concentrated lentivirus solution per 1 million cells. The medium was changed 16 hours after transduction. The lentivirus production was performed as described previously (*21*). Lentiviral packaging (pMD2.G) and envelope (psPAX2) plasmids were provided by D. Trono (École Polytechnique Fédérale de Lausanne, Switzerland). The pCAG-Cre-IRES2-GFP plasmid was a gift from J. Jaworski (International Institute of Molecular and Cell Biology, Warsaw, Poland). The floxed locus was genotyped 3 days after transduction using gDNA isolated from 0.5 million cells with a Genomic Mini kit (A&A Biotechnology). Sequences of primers used for genotyping are listed in table S2. For BMDM stimulation with LPS, on the 14th day after isolation, cells were treated with LPS (100 ng/ml; Santa Cruz Biotechnology, sc3535) for 4 to 16 hours depending on the experiment.

Phylogenetic analysis

Sequences of TENT proteins used for the phylogenetic analysis have been obtained from the WormBase WS272 (*C. elegans*) and UniProt (other organisms), and their IDs are listed in table S4. Sequences were aligned using the PROMALS3D server (*100*). Input sequence alignment for phylogenetic analysis was performed with MUSCLE (*101*). The phylogenetic tree was built using the neighbor-joining method and visualized with iTOL v5 (*102*).

Worms' brood size, body parameters, and locomotion analyses

For brood size analysis, four individual L4 larvae per replicate were placed onto single 35-mm NGM plates seeded with *E. coli* HB101 and were allowed to lay eggs at 20°C. Worms were transferred to fresh plates every 12 hours until they no longer produced embryos. Eggs were counted after the adult was moved. For each strain, 10 worms have been analyzed in two independent trials (two-tailed unpaired *t* test). For worm's body and movement analysis, eight age-synchronized young adult worms per strain were placed onto 35-mm NGM plates seeded with *E. coli*, and the worm movement was recorded for 2 min using the WormLab system (MBF Bioscience). The frame rate, exposure time, and gain were set to 7.5 frames/s, 0.0031 s, and 1, respectively. The worms' body length and width, track length, center point speed, and the overall track pattern of individual worms were analyzed using the WormLab software (MBF Bioscience). For each strain, 80 worms have been analyzed, and data were compared using the two-tailed unpaired Student's *t* test with Welch's correction and presented as mean values ± SD. A $P < 0.05$ was considered significantly different from control: ns, not significant; $*P < 0.05$, $**P < 0.001$, and $***P < 0.0001$.

Microscopic analysis

Worms were immobilized with tetramisole, placed on slides coated with 2% agarose, and immediately imaged. The confocal microscopy for Fig. 1 and fig. S1 was performed using an FV1000 system with a 60×/1.2 water immersion lens (Olympus). Images were processed using Fiji/ImageJ software (version 2.0.0-rc69/1.52p) (*103*). For co-localization analysis presented in Fig. 6, worms were imaged using Zeiss LSM800 confocal microscope with 40×/1.2 water immersion apochromatic objective. Z-stack images were processed using Imaris 8.3 software. Median filter with a 3 × 3 × 1 kernel was applied to remove noise. Analysis was restricted to cells expressing CemOrange2–TRAM-1 ER protein. Gating with polygon was used to exclude the strongest unspecific signal from the green channel (Fig. 6, marked with asterisks). Pearson correlation coefficient was calculated with the ImarisColoc module based on three-dimensional data obtained from 18 worms.

Tethering assay

Tethering assays were performed as previously described (*21*, *104*). 293T cells (American Type Culture Collection, CRL-3216) were cultured in Dulbecco's modified Eagle's medium (Invitrogen) supplemented with 10% FBS (Gibco) and penicillin (100 U/ml)/streptomycin (0.1 mg/ml) (Sigma-Aldrich) at 37°C in 5% CO_2. Cells were seeded into six-well plates and allowed to grow until about 70 to 80% confluence. Next, cells were cotransfected with 0.1 μg of pRL-5Box plasmid carrying an *RL* (*104*) and 2 μg of plasmid encoding tethered wild-type or catalytically inactive NHA–TENT-5 using 5 μl of Lipofectamine 2000 and Opti-MEM medium (Thermo Fisher Scientific, 31985047) according to the manufacturer's instructions. Cells were collected 24 hours after transfection for RNA (Northern blot and DRS) and protein level analyses.

C. elegans cultures for RNA analysis

Animal populations were synchronized by bleaching of the gravid adults and starvation of L1 larvae for 16 hours. Synchronized worms were grown on NGM plates seeded with *E. coli* HB101 at indicated temperatures until they reached the L4 stage. Worms were washed three times with 50 mM NaCl (900*g* for 2 min at room temperature) and resuspended in 1 ml of TRI Reagent (Sigma-Aldrich, T9424). Samples were incubated for 5 min at room temperature and stored at −80°C. For RNA analysis after *C. elegans* infection by *S. aureus*, synchronized worms were grown on NGM plates seeded with *E. coli* HB101 at 25°C until they reached the L4 stage. The infection plates were prepared as described (*37*). Briefly, TSA plates with Nal (10 μg/ml) were prepared 1 week before the experiment and stored at 4°C in the dark. *S. aureus* was grown in TSB + Nal overnight at 37°C. Five hundred microliters of the overnight *S. aureus* culture was uniformly spread onto the entire surface of 100-mm TSA + Nal plates and incubated at 37°C for 6 hours. L4 worms were washed three times

with sterile 50 mM NaCl and seeded onto infection TSA plates that were previously warmed to room temperature. After 8 hours of infection at 25°C, animals were washed off the plates and resuspended in TRI Reagent as described above.

RNA extraction

Total RNA was isolated with TRI Reagent according to the manufacturer's instructions (Sigma-Aldrich, T9424). To ensure the highest purity of the RNA samples isolated from worms, the subsequent phenol/chloroform extraction has been performed according to standard protocols. Before RT-qPCR, RNA-seq and DRS library preparation, RNase H treatment, and PAT total RNA was treated with TURBO DNase (Thermo Fisher Scientific). RNA was then purified by phenol/chloroform extraction and ethanol precipitation.

RNA-seq and data analysis

C. elegans cultures and RNA extraction are described above. Three independent replicate sample sets were prepared for each strain [wild type and *tent-5(tm3504)*] and condition (worms that were grown on *E. coli* HB101 or infected by *S. aureus* for 8 hours). Two micrograms (worms) or 1 μg (wild-type BMDMs stimulated with LPS) of DNase-treated total RNA was used for the library preparation. Ribosomal RNA (rRNA) was removed using a Ribo-Zero rRNA removal kit (human/mouse/rat; Epicentre, RZG1224). Sequencing libraries were prepared using a KAPA stranded RNA-seq library preparation kit (KAPA Biosystems, KR0934), and their quality was assessed with an Agilent 2100 Bioanalyzer (Agilent Technologies Inc.). The libraries were sequenced in the 75-nt single-end (*C. elegans* samples) or 75-nt pair-end (BMDMs) mode on the NextSeq500 Illumina platform. RNA-seq reads were adapter-clipped and quality-filtered with cutadapt (version 1.18) to remove adapters, low-quality fragments (minimum quality score was set to 20), and too short sequences (threshold set to 30 nt) (*105*). Quality-filtered reads were mapped to the respective reference genomes of *C. elegans* (WBCel235; ENSEMBL, release 94) or mouse (GRCm38; ENSEMBL, release 94) using the STAR (Spliced Transcripts Alignment to a Reference) aligner (version 2.6.1b or version 2.7.6a for worm and mouse, respectively) (*106*). Read counts were assigned to genes using featureCounts from the Subread package (version 1.6.3) with options -Q 10 -p -B -C -s 2 -g gene_id -t exon and respective annotation files for *C. elegans* (WBCel235; ENSEMBL, release 94) or mouse (Gencode vM25) (*107*). Multimappers and reads overlapping multiple features were not counted. Differential expression analysis was performed with DESeq2 (version 1.22) Bioconductor package (*108*) with default settings. For *C. elegans*, most of the analyses were performed for the genes, which expression was down-regulated at least 1.5-fold [$\log_2$ fold change < $-\log_2(1.5)$, FDR < 0.05] in mutant worms. Venn diagrams were drawn with VENNY (www.stefanjol.nl/venny). Gene sets were submitted for GO enrichment analysis to the WormBase Enrichment Suite (WS278) (*109*) and WormCat tool (*110*).

DRS and data analysis

For tethering assay, technical replicate sample sets were prepared from 293T cells transfected with the wild-type or catalytically inactive NHA–TENT-5. For *C. elegans* DRS, two independent replicate sample sets were prepared for *tent-5(tm3504)* and wild-type worms [the same input RNA samples as for the RNA-seq experiment (replicates 1 and 2) were used]. For mice samples, BMDMs from *Tent5a*$^{Flox/Flox}$ *Tent5c*$^{-/-}$ and wild-type mice were isolated, cultured, and transduced as described above. On the 14th day after isolation, cells were stimulated with LPS (100 ng/ml) for 8 hours. Two replicate sample sets were prepared from BMDMs for DRS analysis. Total RNA from 293T, *C. elegans*, and BMDM samples was isolated with TRI Reagent according to the manufacturer's instructions (Sigma-Aldrich, T9424). The cap-enriched mRNA was prepared from 100 μg of total RNA with GST-eIF4E^{K119A} protein (homemade) and glutathione sepharose 4B (GE Healthcare, 17-0756-01) as described previously (*23*). Nanopore direct RNA libraries were prepared with a DRS Kit [Oxford Nanopore Technologies (ONT), SQK-RNA002] from 3 μg (worms and 293T) and 3.5 μg (BMDMs) of cap-enriched mRNA mixed with 150 ng of *Saccharomyces cerevisiae* oligothymidilate [oligo(dT)]–enriched mRNA to optimize sequencing efficiency. Sequencing was performed with a MinION device (ONT; Flow cell type FLO-MIN106, RevD). Raw reads were basecalled with the standalone version of Guppy 4.0.11 (ONT). Sequencing reads were mapped to Gencode v36 supplemented with sequences of reporter transcripts (293T), WBCel235 (worms), or Gencode vM26 (BMDMs) reference transcriptomes using MiniMap 2.17 (*111*) with options -k 14 -ax map-ont –secondary = no and processed with samtools 1.9 to filter out supplementary alignments and reads mapping to reverse strand (samtools view -b -F 2320). The poly(A) tail lengths were estimated with Nanopolish (version 0.13.2) polya function (*112*). In subsequent analyses, only length estimates with quality control tag reported by Nanopolish as PASS were considered. Statistical analysis was performed using functions provided in the NanoTail R package (*23*). Poly(A) length distributions in analyzed conditions were compared using the Wilcoxon test, filtering out transcripts that had a low number of supporting reads under each condition (<10). Collected *P* values were adjusted for multiple comparisons using the Benjamini-Hochberg method. Transcripts were considered as having a significant change in poly(A) tail length if the adjusted *P* value was <0.05. Transcripts were considered as TENT-5 or TENT5A/C substrates if, in addition to being significantly changed, their median poly(A) tail length was at least 5 nt shorter in the mutant worms or double *Tent5a*$^{Flox/Flox}$ *Tent5c*$^{-/-}$ mutant compared to wild-type worms or mouse BMDMs, respectively. For differential expression estimates, reads were mapped to *C. elegans* (WBCel235; ENSEMBL, release 94) or mouse (GRCm38; ENSEMBL, release 94) reference genomes using MiniMap 2.17 (*111*), with options -ax splice –secondary = no -uf. Read counts were assigned to genes using featureCounts from the Subread package (version 2.0.1) with options -L –fracOverlap 0.5 –fracOverlapFeature 0.2 -s 1 and respective annotation files for *C. elegans* (WBCel235; ENSEMBL, release 94) or mouse (Gencode vM25) (*107*). Multimappers and reads overlapping multiple features were not counted. Differential expression analysis was performed with DESeq2 (version 1.28) Bioconductor package (*108*) with default settings. Gene sets were submitted for GO enrichment analysis to the WormBase Enrichment Suite (WS278) (*109*) or g:Profiler (*113*).

Transcript and UTR length analysis

Data regarding coordinates of the 5′ and 3′UTRs in the WBCel235 genome and percent guanine-cytosine content for each gene were downloaded from ParaSite BioMart (WS276) (https://parasite.wormbase.org/biomart/martview/). Data regarding transcript and coding sequences lengths were obtained from BioMart using biomaRt R package (biomart = "ensembl" and dataset = "celegans_gene_ensembl"). For each gene, only the longest possible 5′ and 3′UTRs or coding sequence was considered for the analysis. The

lengths of the 5′ and 3′UTRs were calculated on the basis of obtained coordinates. Statistics were calculated using the Wilcoxon test.

Motif enrichment analysis

Data regarding coordinates of the 3′UTRs in the WBCel235 genome were downloaded from ParaSite BioMart (WS276) (https://parasite.wormbase.org/biomart/martview/). Only the longest possible 3′UTR sequence for each gene was considered for the analysis. Coordinates of 3′UTRs of TENT-5 substrates (DRS) and genes that expression levels were down-regulated at least 1.5-fold in *tent-5(tm3505)* mutant worms compared to wild type (RNA-seq), as well as coordinates of 3′UTRs of all remaining genes identified by DRS or RNA-seq (background), were saved as bed file and were used for respective FASTA sequences collection using the bedtools getfasta tool (version 2.29.2) (*114*) and WBCel235 (ENSEMBL, release 94) genome sequence. FASTA sequences of 3′UTRs of TENT5A/C substrates and all Gencode-annotated transcripts in mm10 genome (background) were obtained with bedtools getfasta tool (version 2.29.2) (*114*), using bed files with 3′UTR coordinates downloaded from the UCSC Browser Table tool (Gencode vM23 track and known_gene table) and GRCm38 genome sequence. Sequence motifs were searched using the DREME tool (version 5.3.0) (*59*) with options -rna -norc -k 8 -l with the respective background (described above) specified.

Reverse transcription quantitative polymerase chain reaction

One microgram of the DNase-treated total RNA was reverse-transcribed with 1 μl of oligo(dT)$_{25}$ and random primers mix (50 mM and 50 ng/μl, respectively) using the SuperScript III Reverse Transcriptase (Thermo Fisher Scientific, 18080085). cDNA samples were diluted 10× and used for RT-qPCR analysis using the LightCycler 480 SYBR Green I Master Mix (Roche, 04887352001) and 0.25 μM primers on the LightCycler 480 Instrument (Roche). Primers were designed with Primer-BLAST (National Center for Biotechnology Information) to be exon-junction spanning where possible and tested for amplification efficiencies with a series of template dilutions. Each experimental replicate was measured in technical triplicate. Expression levels for each sample were normalized to *act-1*. Gene expression changes were calculated using the $2^{-\Delta\Delta C(t)}$ method. Unpaired two-sample two-sided *t* test using ΔC_t values were performed for most comparisons except for induction of gene expression during infection, where one-sided *t* tests were performed. A $P < 0.05$ was considered statistically significant: ns, not significant; $^*P \leq 0.05$, $^{**}P \leq 0.01$, and $^{***}P \leq 0.001$. Primer sequences are listed in table S2.

RNase H treatment

Twenty micrograms of DNase-treated total RNA was mixed with 2 μl of 50 mM oligo(dT)$_{25}$, 1 μl 10× hybridization buffer [25 mM tris-HCl (pH 7.5), 1 mM EDTA, and 50 mM NaCl], and water in 10 μl. RNA was denatured at 70°C for 10 min and slowly cooled down to 42°C. Next, 10 μl of prewarmed to 37°C 2× reaction buffer [40 mM tris-HCl (pH 7.5), 20 mM $MgCl_2$, 200 mM KCl, 2 mM DTT, and 10% sucrose] and 1 μl of RNase H (2 U; Thermo Fisher Scientific, EN0201) were added, and the reactions were carried out at 37°C for 1 hour. RNA was recovered with phenol/chloroform extraction, precipitated with 96% ethanol, and analyzed using Northern blots or PAT.

Poly(A) tail analysis

One microgram of DNA-free total RNA was ligated with 125 pmol of RA3_15N 3′ adaptor at 18°C for 16 hours in 20-μl mixtures containing 1× T4 RNA ligase buffer, 10% PEG 8000 (polyethylene glycol, molecular weight 8000), 50 U of RiboLock RNase inhibitor, and 300 U of T4 RNA ligase 2 truncated KQ [New England Biolabs (NEB), M0373L]. The samples were purified with AMPure XP magnetic beads [1:0.75 (v/v) RNA-to-beads ratio] to discard nonligated adapters and short RNA fragments. RNA was eluted in 15 μl of RNase-free water and reverse-transcribed using 200 U of the SuperScript III Reverse Transcriptase (Thermo Fisher Scientific) and 100 pmol of the RPI PCR Index Primer (TruSeq Illumina) according to the manufacturer's protocol. The cDNAs were purified using AMPure XP beads [1:1 (v/v) ratio], eluted with 20 μl of RNase-free water, and used for the nested PCR. Briefly, 1 μl of the cDNA was used for PCR-1 (Phusion Hot Start II; 25 cycles), with a gene-specific forward primer and a universal reverse primer RPuni. The PCR-1 samples were diluted 100× and used as a template for PCR-2, with a second forward gene-specific primer and RPuni. The PCR-1 and PCR-2 amplicons were analyzed in the 2% agarose gels in 1× TBE buffer (90 mM tris-borate and 2 mM EDTA). All primers used for PAT are described in table S2.

Northern blotting

High-molecular weight RNA samples were separated on 1.2% agarose gels containing 1.7% formaldehyde in 1× NBC buffer (50 mM boric acid, 1 mM sodium acetate, and 5 mM NaOH) and transferred to Hybond-N+ membranes (GE Healthcare) by overnight capillary elution using 8× SSC buffer (1.2 M NaCl and 120 mM sodium citrate). Low–molecular weight RNA samples were separated on 4 to 6% acrylamide gels containing 7 M urea in 0.5× TBE buffer (45 mM tris-borate and 1 mM EDTA) and electrotransferred to membranes in 0.5× TBE buffer at 300 to 350 mA at 4°C for 3 hours. RNA was immobilized on membranes by 254-nm UV light using a CL-1000 cross-linker (UVP) with the auto cross-link function (120 mJ/cm^2). Next, membranes were stained with 0.03% methylene blue in 0.3 M NaAc (pH 5.3), and staining was digitized. Random primed *RL* probes were PCR-amplified with primers RL_Fw and RL_Rev using pRL-5Box plasmid as a template and radioactively labeled with 20 μCi of [α-^{32}P]-dATP and the DECAprime II DNA Labeling Kit (Thermo Fisher Scientific, AM1456). Membranes were prehybridized in the PerfectHyb Plus Hybridization Buffer (Sigma-Aldrich) at 65°C for 30 min and incubated with probes in PerfectHyb buffer at 65°C overnight with rotation. Membranes were washed three times in prewarmed 0.5× SSC with 0.1% SDS at 65°C for 20 min and then exposed overnight to PhosphorImager screens (Fujifilm). The screens were scanned with a Typhoon FLA 7000 scanner (GE Healthcare) and analyzed with Multi Gauge software version 2.0 (Fujifilm).

Subcellular protein fractionation

Mixed-stage worm populations were grown on NGM plates seeded with *E. coli* HB101 at 20°C. Two independent replicate sample sets were prepared for each strain. Subcellular protein fractionation was performed using the Subcellular Protein Fractionation Kit (Thermo Fisher Scientific, 78840). Briefly, all buffers were supplemented with protease inhibitors (Invitrogen), and the entire procedure was performed at 4°C. For each strain, worms were washed from three 100-mm plates and washed three times with 50 mM NaCl (900*g* for 2 min at room temperature). Worms were resuspended in ice-cold 1.5 ml of cytoplasmic extraction buffer and lysed using Omni tissue homogenizer for 1 min following 10 min of incubation with

gentle mixing. Lysates were centrifuged at 500*g*, and the supernatant was collected as a cytoplasmic fraction, while the pellet was resuspended in membrane extraction buffer. After 10 min of incubation, the sample was centrifuged at 3000*g*, and the supernatant was collected as a membrane fraction. Last, the pellet was resuspended in nuclear extraction buffer, incubated for 30 min, and centrifuged at 5000*g*. The supernatant was collected as a nuclear fraction. The concentration of protein was measured by Bradford assay, and samples for SDS-PAGE and Western blot were prepared using the same amount of protein from each fraction. Control total protein input samples were prepared by boiling worms in 1× SDS sample buffer.

Total worm extract preparation for Superdex 200 chromatography

Protein extracts were prepared from mixed-stage worm populations grown at 20°C. Animals were washed three times with 50 mM NaCl and then briefly with lysis buffer [50 mM Hepes (pH 7.4), 100 mM NaCl, 3 mM $MgCl_2$, 0.5 mM DTT, 0.05% NP-40 substitute, and 10% (v/v) glycerol]. The supernatant was discarded, and the pellet was resuspended in 5 V of lysis buffer supplemented with 1 mM phenylmethylsulfonyl fluoride (PMSF), 1× chymostatin, and 1× protease inhibitors and drop-frozen in liquid nitrogen. Lysis was performed by grinding frozen worms in liquid nitrogen. The extract was allowed to melt on ice and supplemented with 1 mM PMSF, 1× chymostatin, and 1×protease inhibitors. The lysate was cleared by two centrifugation steps at 20,000*g* at 4°C for 20 min. Five hundred microliters of the lysate (7 μg/μl) was subjected to the Superdex 200 chromatography column equilibrated with lysis buffer. Two hundred microliters of each collected fraction was precipitated using methanol/chloroform; pellets were resuspended in 20 μl of 1× SDS sample buffer, boiled, and used for the SDS-PAGE and Western blot.

Western blotting

BMDMs from *Tent5a*$^{Flox/Flox}$ *Tent5c*$^{-/-}$, *Tent5a*-3xFLAG, *Tent5c*-3xFLAG, and wild-type mice were isolated, cultured, and transduced as described above. On the 13th day after isolation, cells were counted and seeded on six-well plates, with 0.5 million cells per well. The next day, cells were stimulated with LPS (100 ng/ml) for 8 hours (*Tent5a*$^{Flox/Flox}$ *Tent5c*$^{-/-}$ and wild type) or for 0 to 16 hours of time points (*Tent5a*-3xFLAG, *Tent5c*-3xFLAG, and wild type). BMDMs were scratched and pelleted by centrifugation for 3 min at 350*g*. Cells were lysed with 0.1% NP-40 in phosphate-buffered saline (PBS) supplemented with protease inhibitors and viscolase (final concentration of 0.1 U/ml; A&A Biotechnology). The samples were incubated at 37°C for 30 min with shaking before 3× SDS sample buffer [187.5 mM tris-HCl (pH 6.8), 6% SDS, 150 mM DTT, 0.02% bromophenol blue, 30% glycerol, and 3% 2-mercaptoethanol] was added, and the lysates were boiled for 10 min. Lysates from the 293T cells following tethering assay were prepared using the same protocol. Protein samples from a mixed population of worms were prepared by boiling ~100 worms in 3× SDS sample buffer for 5 min. Boiled protein mixtures from cells or worms were cleared by centrifugation for 5 min at maximum speed at room temperature and resolved on 10 to 12% SDS-PAGE gels. Proteins were transferred to Protran nitrocellulose membranes (GE Healthcare) by wet transfer at 300 mA at 4°C for 2 hours in 1× transfer buffer [25 mM tris base, 192 mM glycine, and 20% methanol (v/v)]. After transfer, the membranes were stained with 0.3% (w/v) Ponceau S in 3% (v/v) acetic acid, and the staining was digitized. Next, membranes were soaked in 5% (w/v) nonfat milk in 1× TBS-T (20 mM tris base, 150 mM NaCl, and 0.01% Tween 20) for 1 hour with gentle agitation at room temperature, followed by the overnight incubation at 4°C with specific primary antibodies diluted 1:3000 (anti-*RL* antibody, clone 5B11.2; Millipore, MAB4400), 1:3000 (GFP B-2; Santa Cruz Biotechnology, sc-9996), 1:1000 (FLAG; Proteintech, 20543-1-AP), 1:10,000 RFP (red fluorescent protein); Erdogan, AB233), 1:5000 [glyceraldehyde phosphate dehydrogenase (GAPDH); Proteintech, 10494-1-AP], 1:10,000 (α-tubulin, clone DM1A; Millipore, MABT205), 1:1000 (iNOS; Cell Signaling Technology, 13120), 1:1000 (CD80; Cell Signaling Technology, 54521), 1:30,000 (lysozyme; Abcam, ab108508), 1:30,000 (cathepsin S; Invitrogen, MA5-29695), 1:10,000 (cathepsin B; Abcam, ab214428), and 1:20,000 (cathepsin D; Abcam, ab75852). Membranes were washed three times for 10 min each in 1× TBS-T and then incubated for 2 hours with gentle agitation at room temperature with horseradish peroxidase–conjugated secondary anti-mouse (Millipore, 401215) or anti-rabbit (Millipore, 401393) antibodies diluted 1:5000. Following three washes in 1× TBS-T, blots were incubated with the Clarity Western ECL Substrate (Bio-Rad) for 1 to 3 min, and signals were detected either through exposure to a CL-Exposure film (Thermo Fisher Scientific) and developed in an AGFA Curix CP-1000 device or visualized using the ChemiDoc Imaging System (Bio-Rad). Protein bands from Western blots were quantified with ImageJ as described in www.yorku.ca/yisheng/Internal/Protocols/ImageJ.pdf. Final relative quantification values represent the ratio of net band intensity from the protein of interest to net GAPDH (loading control).

Mass spectrometry

Protein extracts were prepared in eight replicate sample sets. The *tent-5(tm3504)* mutant and wild-type worms were grown at 20°C on *E. coli* HB101 until they reached the L4 stage. Worms were washed three times with 50 mM NaCl and once in 1× lysis buffer [50 mM Hepes (pH 7.4), 100 mM NaCl, 3 mM $MgCl_2$, 0.5 mM DTT, 0.05% NP-40 substitute, and 10% (v/v) glycerol]. Pellets were resuspended in 900 μl of 1× lysis buffer supplemented with 1 mM PMSF, 1× chymostatin, and 1× protease inhibitors; transferred to 2-ml tubes containing 200 μl of Zirconia beads (BioSpec Products); and drop-frozen in liquid nitrogen. Next, tubes were inserted into the Fast Prep-24 machine (MP Biomedicals), and worms were crushed for 1 min at maximum speed. Following centrifugation at 14,000*g* for 10 min at 4°C, lysates were transferred to the new tubes and subjected to sonication at high amplitude for 20 min (30-s on/30-s off cycle) (Diagenode Bioruptor XL) and then cleared by centrifugation at 14,000*g* for 30 min at 4°C. A Millipore Direct Detect infrared spectrometer was used to determine the total protein concentration of the lysate. Sample preparation was done on the basis of modified FASP (Filter-aided sample preparation) protocol (*115*). Briefly, a supernatant was placed at Vivacon 30-kDa filter (Sartorius), centrifuged, and washed three times with 200 μl of 8 M urea in 100 mM NH_4HCO_3. Next, samples were reduced (DTT at room temperature for 30 min) and alkylated (indole-3-acetic acid at room temperature for 15 min) following overnight digestion with trypsin (Promega) and acidified with trifluoroacetic acid to a final concertation of 0.1%. Mass spectrometry (MS) analysis was performed by liquid chromatography–MS in the Laboratory of Mass Spectrometry (Institute of Biochemistry and Biophysics, Polish Academy of Sciences, Warsaw) using a nanoACQUITY UPLC system (Waters, 176016000) coupled to an LTQ-Orbitrap Velos mass spectrometer (Thermo Fisher

Scientific). Peptides were separated by a 180-min linear gradient of 95% solution A (0.1% formic acid in water) to 35% solution B (acetonitrile and 0.1% formic acid). The measurement of each sample was preceded by three washing runs to avoid cross-contamination; the final MS washing run was searched for the presence of cross-contamination between samples. If the protein of interest was identified in the washing run and the next measured sample at the same or smaller intensity, then the sample was regarded as contaminated and excluded from the final graphs. The mass spectrometer was operated in the data-dependent MS-MS2 mode, and data were acquired in the mass/charge ratio range of 300 to 2000. MS raw data files were used to calculate protein abundance in the samples using the MaxQuant (version 1.6.3.4) platform (*116*). The reference proteome of *C. elegans* database from UniProt (27,805 protein entries) and common contaminates list included in MaxQuant were used, and analysis was performed with the following settings: match between runs, variable modification: oxidation (M), and 4.5 parts per million of error tolerance. Label-free quantification (LFQ) intensity values were calculated using the MaxLFQ algorithm to estimate quantities of identified proteins. Protein abundance was defined as the LFQ value calculated by MaxQuant software for a protein (sum of intensities of identified peptides of a given protein) divided by its molecular weight. The Scafold4 Q + S platform was used for statistical analysis. Protein abundance in analyzed samples was compared using the Mann-Whitney test with Benjamini-Hochberg correction.

Life-span and killing assays

The 35-mm plates with TSA + Nal (final concentration of 10 μg/ml) for killing assays on *S. aureus* NCTC8325 were prepared 1 week before the experiments and stored at 4°C protected from light (*37*). Survival analysis on *S. marcescens* Db10, *P. luminescens*, and respective control *E. coli* OP50 were performed on the 35-mm plates with NGM without the addition of drugs or antibiotics. Life-span assays on *E. coli* HB101, *P. aeruginosa* PAO1, and some assays on *E. coli* OP50 were performed with the addition of FUdR (5-Fluoro-2′-deoxyuridine) (final concentration of 0.1 mg/ml; Sigma-Aldrich, F0503) to prevent progeny production. All bacteria strains were freshly seeded from the −80°C stock 3 days before an experiment to the appropriate solid medium. *E. coli* OP50 was cultured overnight in LB, and 50 μl of overnight culture was spread onto the center of 35-mm NGM plates and incubated at 37°C for 16 hours. *E. coli* HB101 was cultured overnight in LB + streptomycin (0.1 mg/ml). Fifty microliters of overnight culture was spread onto the center of 35-mm NGM or NGM + FUdR plates (depending on the experiment setup) and incubated at 37°C for 16 hours. For survival analysis on UV-killed *E. coli* HB101, NGM + FUdR plates seeded with bacteria were exposed to UV light in a UV Stratalinker 2400 for 30 min at maximum. For survival analysis on heat-killed bacteria, *E. coli* HB101 and OP50 were cultured overnight in 50 ml of LB and centrifuged at 7000*g* for 10 min at room temperature, and pellets were resuspended in 5 ml of fresh LB. Next, to kill bacteria, mixtures were incubated in the water bath at 65°C for 30 min. Fifty microliters of culture containing dead bacteria was spread onto the center of 35-mm plates and incubated at 25°C for 24 hours. Bacterial killing was evaluated by inoculating LB medium with UV- or heat-treated bacteria, and lack of growth at 37°C confirmed effective killing. *S. aureus* was grown overnight in TSB + Nal (10 μg/ml). Ten microliters of overnight culture was spread onto the center of 35-mm TSA + Nal plates and incubated at 37°C for 6 hours and then cooled down to 25°C and used for the killing assays. *P. aeruginosa* and *S. marcescens* were grown overnight at 37°C in LB. Ten microliters of overnight cultures was spread onto the center of 35-mm NGM or NGM + FUdR plates (for *S. marcescens* and *P. aeruginosa*, respectively) and incubated at 37°C for 24 hours and then at 25°C for another 24 hours. *P. luminescens* was cultured overnight at 30°C in LB, and 10 μl of the overnight culture was spread onto the center of 35-mm NGM plates and incubated at 30°C for 24 hours and after that at 25°C for 24 hours. All worms were grown on NGM + *E. coli* HB101 at 20° or 25°C (depending on the temperature in which the assays were performed) for three to four generations before the experiments. Animal populations were synchronized by bleaching of the gravid adults and the starvation of L1 larvae for 16 hours at appropriate temperatures. Forty to 60 L4-staged worms were transferred to each of the three replicate assay plates per strain. Beginning on the next day, the number of dead and live worms on each plate was recorded daily (*S. marcescens*, *P. aeruginosa*, *P. luminescens*, and *E. coli*) or twice a day (*S. aureus*). Live worms were transferred daily to new plates to avoid contamination with the progeny (*S. marcescens*, *P. luminescens*, and related *E. coli* OP50 control). For *P. aeruginosa* tests, worms were not transferred to the new plates. For *E. coli* HB101 life spans performed on the NGM + FUdR plates, worms were transferred to the new plates every 3 days until day 12 and then left on the same plates. Worms that left the plates in the first several days of the assay were removed from the counts of subsequent days. Animals were considered dead if they failed to respond to a gentle touch. For each survival experiment, at least two biological replicates were carried out. Kaplan-Meier survival analyses were performed using GraphPad Prism 7 software. Life-span survival data were compared using the log-rank significance test and presented as median survival. A $P < 0.05$ was considered significantly different from control: ns, not significant; $^{*}P < 0.05$, $^{**}P < 0.01$, $^{***}P < 0.001$, and $^{****}P < 0.0001$.

CFU assays

Exposure of wild-type and mutant worms to *E. coli* HB101 and *P. aeruginosa* PAO1 was carried out exactly as for life-span and killing assays described above. CFU assays were performed essentially as described in (*49*, *50*) with minor modifications. Briefly, on the 5th (HB101) and 4th (PAO1) day of adulthood, 30 worms of each genotype from each of the three technical replicate plates were collected into 50 μl of 1× M9 supplemented with 25 mM levamisole (Sigma-Aldrich, L9756) to inhibit pharyngeal pumping and expulsion. Worms were washed in 1× M9 + 25 mM levamisole three times and then surface-sterilized in 1× M9 + 25 mM levamisole + kanamycin (100 μg/ml) for 45 min at room temperature. Following three washes with 1× M9 + 25 mM levamisole, worms were resuspended in 150 μl of PBS containing 0.1% Triton X-100. A 100-μl aliquot of the supernatant was removed from each replicate to test for external bacterial contamination. Animals were homogenized in the remaining 50 μl of PBS + 0.1% Triton X-100 with pellet pestle (Bel-Art, BAF199230001) and motor for 30 s, and then 450 μl of PBS was added to each sample. Dilution series of homogenates was spread to the LB plates without antibiotics and grown at 37°C for 24 hours. CFU value per worm was counted as follows: number of CFU/worm = (number of colonies × dilution factor)/number of worms in lysate − external CFU. For each CFU experiment, three biological replicates were carried out, each comprising at least two technical replicates. A $P < 0.05$ was considered significantly different from control: ns, not significant; $^{*}P < 0.05$ and $^{**}P < 0.01$.

Statistical analysis

Statistical analysis was performed in Microsoft Excel (RT-qPCR), GraphPad Prism 7 (life span assays), or with R 4.0 (*117*). Details of the particular statistical analyses, significance, number of replicates and sample sizes, and the features of all plots are described in the figure legends. Data plotted as box plots have the following features: whiskers (25th and 75th percentiles), minima and maxima (5th and 95th percentiles), and thick lines (median). Data presented as heatmaps were normalized to a sequencing depth using DESeq2 and transformed with regularized log transformation for visualization purposes.

SUPPLEMENTARY MATERIALS

Supplementary material for this article is available at https://science.org/doi/10.1126/sciadv.add9468

View/request a protocol for this paper from *Bio-protocol*.

REFERENCES AND NOTES

1. J. A. Hoffmann, F. C. Kafatos, C. A. Janeway, R. A. B. Ezekowitz, Phylogenetic perspectives in innate immunity. *Science* **284**, 1313–1318 (1999).
2. A. Iwasaki, R. Medzhitov, Control of adaptive immunity by the innate immune system. *Nat. Immunol.* **16**, 343–353 (2015).
3. K. Buchmann, Evolution of innate immunity: Clues from invertebrates via fish to mammals. *Front. Immunol.* **5**, 1–8 (2014).
4. D. H. Kim, J. J. Ewbank, Signaling in the innate immune response. *WormBook* **2018**, 1–35 (2018).
5. J. E. Irazoqui, J. M. Urbach, F. M. Ausubel, Evolution of host innate defence: Insights from *Caenorhabditis elegans* and primitive invertebrates. *Nat. Rev. Immunol.* **10**, 47–58 (2010).
6. G. Gasteiger, A. D'osualdo, D. A. Schubert, A. Weber, E. M. Bruscia, D. Hartl, Cellular innate immunity: An old game with new players. *J. Innate Immun.* **9**, 111–125 (2017).
7. S. Carpenter, E. P. Ricci, B. C. Mercier, M. J. Moore, K. A. Fitzgerald, Post-transcriptional regulation of gene expression in innate immunity. *Nat. Rev. Immunol.* **14**, 361–376 (2014).
8. Y. Shi, J. L. Manley, The end of the message: Multiple protein–RNA interactions define the mRNA polyadenylation site. *Genes Dev.* **29**, 889–897 (2015).
9. J. Neve, R. Patel, Z. Wang, A. Louey, A. M. Furger, Cleavage and polyadenylation: Ending the message expands gene regulation. *RNA Biol.* **14**, 865–890 (2017).
10. A. L. Jalkanen, S. J. Coleman, J. Wilusz, Determinants and implications of mRNA poly(A) tail size—Does this protein make my tail look big? *Semin. Cell Dev. Biol.* **34**, 24–32 (2014).
11. Y. Bin Yan, Deadenylation: Enzymes, regulation, and functional implications. *Wiley Interdiscip. Rev. RNA* **5**, 421–443 (2014).
12. G. Martin, W. Keller, RNA-specific ribonucleotidyl transferases. *RNA* **13**, 1834–1849 (2007).
13. S. Yu, V. N. Kim, A tale of non-canonical tails: gene regulation by post-transcriptional RNA tailing. *Nat. Rev. Mol. Cell Biol.* **21**, 542–556 (2020).
14. V. Liudkovska, A. Dziembowski, Functions and mechanisms of RNA tailing by metazoan terminal nucleotidyltransferases. *Wiley Interdiscip. Rev. RNA* **12**, e1622 (2021).
15. J. H. Kim, J. D. Richter, Opposing polymerase-deadenylase activities regulate cytoplasmic polyadenylation. *Mol. Cell* **24**, 173–183 (2006).
16. K. W. Kim, T. L. Wilson, J. Kimble, GLD-2/RNP-8 cytoplasmic poly(A) polymerase is a broad-spectrum regulator of the oogenesis program. *Proc. Natl. Acad. Sci. U.S.A.* **107**, 17445–17450 (2010).
17. M. Nousch, A. Yeroslaviz, C. R. Eckmann, Stage-specific combinations of opposing poly(A) modifying enzymes guide gene expression during early oogenesis. *Nucleic Acids Res. Res.* **47**, 10881–10893 (2019).
18. E. K. Jae, E. Drier, S. A. Barbee, M. Ramaswami, J. C. P. Yin, M. Wickens, GLD2 poly(A) polymerase is required for long-term memory. *Proc. Natl. Acad. Sci. U.S.A.* **105**, 14644–14649 (2008).
19. T. Udagawa, S. A. Swanger, K. Takeuchi, J. H. Kim, V. Nalavadi, J. Shin, L. J. Lorenz, R. S. Zukin, G. J. Bassell, J. D. Richter, Bidirectional control of mRNA translation and synaptic plasticity by the cytoplasmic polyadenylation complex. *Mol. Cell* **47**, 253–266 (2012).
20. K. Kuchta, A. Muszewska, L. Knizewski, K. Steczkiewicz, L. S. Wyrwicz, K. Pawlowski, L. Rychlewski, K. Ginalski, FAM46 proteins are novel eukaryotic non-canonical poly(A) polymerases. *Nucleic Acids Res.* **44**, 3534–3548 (2016).
21. S. Mroczek, J. Chlebowska, T. M. Kuliński, O. Gewartowska, J. Gruchota, D. Cysewski, V. Liudkovska, E. Borsuk, D. Nowis, A. Dziembowski, The non-canonical poly(A) polymerase *FAM46C* acts as an onco-suppressor in multiple myeloma. *Nat. Commun.* **8**, 619 (2017).
22. Y. X. Zhu, C. X. Shi, L. A. Bruins, P. Jedlowski, X. Wang, K. M. Kortüm, M. Luo, J. M. Ahmann, E. Braggio, A. K. Stewart, Loss of *FAM46C* promotes cell survival in myeloma. *Cancer Res.* **77**, 4317–4327 (2017).
23. A. Bilska, M. Kusio-kobia, P. S. Krawczyk, O. Gewartowska, B. Tarkowski, K. Koby, D. Nowis, J. Golab, J. Gruchota, E. Borsuk, A. Dziembowski, S. Mroczek, Immunoglobulin expression and the humoral immune response is regulated by the non-canonical poly(A) polymerase TENT5C. *Nat. Commun.* **11**, 1–17 (2020).
24. A. B. Herrero, D. Quwaider, L. A. Corchete, M. V. Mateos, R. García-Sanz, N. C. Gutiérrez, FAM46C controls antibody production by the polyadenylation of immunoglobulin mRNAs and inhibits cell migration in multiple myeloma. *J. Cell. Mol. Med.* **00**, 1–12 (2020).
25. J. L. Hu, H. Liang, H. Zhang, M. Z. Yang, W. Sun, P. Zhang, L. Luo, J. X. Feng, H. Bai, F. Liu, T. Zhang, J. Y. Yang, Q. Gao, Y. Long, X. Y. Ma, Y. Chen, Q. Zhong, B. Yu, S. Liao, Y. Wang, Y. Zhao, M. S. Zeng, N. Cao, J. Wang, W. Chen, H. T. Yang, S. Gao, FAM46B is a prokaryotic-like cytoplasmic poly(A) polymerase essential in human embryonic stem cells. *Nucleic Acids Res.* **48**, 2733–2748 (2020).
26. O. Gewartowska, G. Aranaz-Novaliches, P. S. Krawczyk, S. Mroczek, M. Kusio-Kobiałka, B. Tarkowski, F. Spoutil, O. Benada, O. Kofroňová, P. Szwedziak, D. Cysewski, J. Gruchota, M. Szpila, A. Chlebowski, R. Sedlacek, J. Prochazka, A. Dziembowski, Cytoplasmic polyadenylation by TENT5A is required for proper bone formation. *Cell Rep.* **35**, 109015 (2021).
27. J. Coller, M. Wickens, Tethered function assays: An adaptable approach to study RNA regulatory proteins. *Methods Enzymol.* **429**, 299–321 (2007).
28. E. R. Troemel, S. W. Chu, V. Reinke, S. S. Lee, F. M. Ausubel, D. H. Kim, p38 MAPK regulates expression of immune response genes and contributes to longevity in *C. elegans*. *PLOS Genet.* **2**, 1725–1739 (2006).
29. T. Roeder, M. Stanisak, C. Gelhaus, I. Bruchhaus, J. Grötzinger, M. Leippe, Caenopores are antimicrobial peptides in the nematode *Caenorhabditis elegans* instrumental in nutrition and immunity. *Dev. Comp. Immunol.* **34**, 203–209 (2010).
30. H. Schulenburg, M. P. Hoeppner, J. Weiner, E. Bornberg-Bauer, Specificity of the innate immune system and diversity of C-type lectin domain (CTLD) proteins in the nematode *Caenorhabditis elegans*. *Immunobiology* **213**, 237–250 (2008).
31. I. Engelmann, A. Griffon, L. Tichit, F. Montañana-Sanchis, G. Wang, V. Reinke, R. H. Waterston, L. D. W. Hillier, J. J. Ewbank, A comprehensive analysis of gene expression changes provoked by bacterial and fungal infection in *C. elegans*. *PLOS ONE* **6**, e19055 (2011).
32. C. Taffoni, N. Pujol, Mechanisms of innate immunity in *C. elegans* epidermis. *Tissue Barriers* **3**, 1–8 (2015).
33. J. H. Thomas, Concerted evolution of two novel protein families in *Caenorhabditis species*. *Genetics* **172**, 2269–2281 (2006).
34. D. Wong, D. Bazopoulou, N. Pujol, N. Tavernarakis, J. J. Ewbank, Genome-wide investigation reveals pathogen-specific and shared signatures in the response of *Caenorhabditis elegans* to infection. *Genome Biol.* **8**, R194 (2007).
35. G. V. Mallo, C. L. Kurz, C. Couillault, N. Pujol, S. Granjeaud, Y. Kohara, J. J. Ewbank, Inducible antibacterial defense system in *C. elegans*. *Curr. Biol.* **12**, 1209–1214 (2002).
36. C. T. Murphy, S. A. McCarroll, C. I. Bargmann, A. Fraser, R. S. Kamath, J. Ahringer, H. Li, C. Kenyon, Genes that act downstream of DAF-16 to influence the lifespan of *Caenorhabditis elegans*. *Nature* **424**, 277–283 (2003).
37. O. Visvikis, N. Ihuegbu, S. A. Labed, L. G. Luhachack, A. M. F. Alves, A. C. Wollenberg, L. M. Stuart, G. D. Stormo, J. E. Irazoqui, Innate host defense requires TFEB-mediated transcription of cytoprotective and antimicrobial genes. *Immunity* **40**, 896–909 (2014).
38. A. Sinha, R. Rae, I. Iatsenko, R. J. Sommer, System wide analysis of the evolution of innate immunity in the nematode model species *Caenorhabditis elegans* and *Pristionchus pacificus*. *PLOS ONE* **7**, e44255 (2012).
39. S. Alper, S. J. McBride, B. Lackford, J. H. Freedman, D. A. Schwartz, Specificity and complexity of the *Caenorhabditis elegans* innate immune response. *Mol. Cell. Biol.* **27**, 5544–5553 (2007).
40. W. Yang, K. Dierking, P. C. Rosenstiel, H. Schulenburg, GATA transcription factor as a likely key regulator of the *Caenorhabditis elegans* innate immune response against gut pathogens. *Fortschr. Zool.* **119**, 244–253 (2016).
41. E. A. Evans, T. Kawli, M. W. Tan, Pseudomonas aeruginosa suppresses host immunity by activating the DAF-2 insulin-like signaling pathway in *Caenorhabditis elegans*. *PLOS Pathog.* **4**, e1000175 (2008).
42. R. P. Shivers, M. J. Youngman, D. H. Kim, Transcriptional responses to pathogens in *Caenorhabditis elegans*. *Curr. Opin. Microbiol.* **11**, 251–256 (2008).
43. X. X. Lin, I. Sen, G. E. Janssens, X. Zhou, B. R. Fonslow, D. Edgar, N. Stroustrup, P. Swoboda, J. R. Yates, G. Ruvkun, C. G. Riedel, DAF-16/FOXO and HLH-30/TFEB function as combinatorial transcription factors to promote stress resistance and longevity. *Nat. Commun.* **9**, 4400 (2018).
44. D. Gems, D. L. Riddle, Genetic, behavioral and environmental determinants of male longevity in *Caenorhabditis elegans*. *Genetics* **154**, 1597–1610 (2000).

45. D. Garigan, A. L. Hsu, A. G. Fraser, R. S. Kamath, J. Abringet, C. Kenyon, Genetic analysis of tissue aging in *Caenorhabditis elegans*: A role for heat-shock factor and bacterial proliferation. *Genetics* **161**, 1101–1112 (2002).
46. J. E. Irazoqui, E. R. Troemel, R. L. Feinbaum, L. G. Luhachack, B. O. Cezairliyan, F. M. Ausubel, Distinct pathogenesis and host responses during infection of *C. elegans* by *P. aeruginosa* and *S. aureus*. *PLOS Pathog.* **6**, 1–24 (2010).
47. C. L. Kurz, S. Chauvet, E. Andrès, M. Aurouze, I. Vallet, G. P. F. Michel, M. Uh, J. Celli, A. Filloux, S. De Bentzmann, I. Steinmetz, J. A. Hoffmann, B. B. Finlay, J.-P. Gorvel, D. Ferrandon, J. J. Ewbank, Virulence factors of the human opportunistic pathogen *Serratia marcescens* identified by in vivo screening. *EMBO J.* **22**, 1451–1460 (2003).
48. C. Couillault, J. J. Ewbank, Diverse bacteria are pathogens of *Caenorhabditis elegans*. *Infect. Immun.* **70**, 4705–4707 (2002).
49. M. F. Palominos, A. Calixto, Quantification of bacteria residing in *Caenorhabditis elegans* intestine. *Bio Protoc.* **10**, 1–12 (2020).
50. F. Rodriguez Ayala, S. Cogliati, C. Bauman, C. Leñini, M. Bartolini, J. Villalba, F. Argañaraz, R. Grau, Culturing bacteria from *Caenorhabditis elegans* gut to assess colonization proficiency. *Bio Protoc.* **7**, e2345 (2017).
51. M. E. Hoinville, A. C. Wollenberg, Changes in *Caenorhabditis elegans* gene expression following exposure to *Photorhabdus luminescens* strain TT01. *Dev. Comp. Immunol.* **82**, 165–176 (2018).
52. I. Legnini, J. Alles, N. Karaiskos, S. Ayoub, N. Rajewsky, FLAM-seq: Full-length mRNA sequencing reveals principles of poly(A) tail length control. *Nat. Methods* **16**, 879–886 (2019).
53. S. A. Lima, L. B. Chipman, A. L. Nicholson, Y. H. Chen, B. A. Yee, G. W. Yeo, J. Coller, A. E. Pasquinelli, Short poly(A) tails are a conserved feature of highly expressed genes. *Nat. Struct. Mol. Biol.* **24**, 1057–1063 (2017).
54. J. Tao, Y. Hao, X. Li, H. Yin, X. Nie, J. Zhang, B. Xu, Q. Chen, B. Li, Systematic identification of housekeeping genes possibly used as references in *Caenorhabditis elegans* by large-scale data integration. *Cells* **9**, 786 (2020).
55. C. Y. Ewald, J. N. Landis, J. P. Abate, C. T. Murphy, T. K. Blackwell, Dauer-independent insulin/IGF-1-signalling implicates collagen remodelling in longevity. *Nature* **519**, 97–101 (2015).
56. D. Sellegounder, Y. Liu, P. Wibisono, C. H. Chen, D. Leap, J. Sun, Neuronal GPCR NPR-8 regulates *C. elegans* defense against pathogen infection. *Sci. Adv.* **5**, eaaw4717 (2019).
57. Y. Liu, D. Martinez-Martinez, C. L. Essmann, M. R. Cruz, F. Cabreiro, D. A. Garsin, Transcriptome analysis of *Caenorhabditis elegans* lacking heme peroxidase SKPO-1 reveals an altered response to *Enterococcus faecalis*. *G3 (Bethesda)* **11**, jkaa055 (2021).
58. I. Gallotta, A. Sandhu, M. Peters, M. Haslbeck, R. Jung, S. Agilkaya, J. L. Blersch, C. Rödelsperger, W. Röseler, C. Huang, R. J. Sommer, D. C. David, Extracellular proteostasis prevents aggregation during pathogenic attack. *Nature* **584**, 410–414 (2020).
59. T. L. Bailey, DREME: Motif discovery in transcription factor ChIP-seq data. *Bioinformatics* **27**, 1653–1659 (2011).
60. J. Suh, H. Hutter, A survey of putative secreted and transmembrane proteins encoded in the *C. elegans* genome. *BMC Genomics* **13**, 333 (2012).
61. J. D. McGhee, The Caenorhabditis elegans intestine. *Wiley Interdiscip. Rev. Dev. Biol.* **2**, 347–367 (2013).
62. C. Coburn, D. Gems, The mysterious case of the *C. elegans* gut granule: Death anthranilic acid and the kynurenine pathway. *Front. Genet.* **4**, 151 (2013).
63. B. J. Thomas, I. E. Wight, W. Y. Y. Chou, M. Moreno, Z. Dawson, A. Homayouni, H. Huang, H. Kim, H. Jia, J. R. Buland, J. A. Wambach, F. S. Cole, S. C. Pak, G. A. Silverman, C. J. Luke, CemOrange2 fusions facilitate multifluorophore subcellular imaging in *C. elegans*. *PLOS ONE* **14**, 1–25 (2019).
64. C. Fucci, M. Resnati, E. Riva, T. Perini, E. Ruggieri, U. Orfanelli, F. Paradiso, F. Cremasco, A. Raimondi, E. Pasqualetto, M. Nuvolone, L. Rampoldi, S. Cenci, E. Milan, The interaction of the tumor suppressor FAM46C with p62 and FNDC3 proteins Integrates protein and secretory homeostasis. *Cell Rep.* **32**, 108162 (2020).
65. N. Manfrini, M. Mancino, A. Miluzio, S. Oliveto, M. Balestra, P. Calamita, R. Alfieri, R. L. Rossi, M. Sassoe-Pognetto, C. Salio, A. Cuomo, T. Bonaldi, M. Manfredi, E. Marengo, E. Ranzato, S. Martinotti, D. Cittaro, G. Tonon, S. Biffo, FAM46C and FNDC3A are multiple myeloma tumor suppressors that act in concert to impair clearing of protein aggregates and autophagy. *Cancer Res.* **80**, 4693–4706 (2020).
66. R. A. Zabinsky, B. M. Weum, M. Cui, M. Han, RNA binding protein vigilin collaborates with miRNAs to regulate gene expression for *Caenorhabditis elegans* larval development. *G3 (Bethesda)* **7**, 2511–2518 (2017).
67. Y. S. Ooi, K. Majzoub, R. A. Flynn, M. A. Mata, J. Diep, J. K. Li, N. van Buuren, N. Rumachik, A. G. Johnson, A. S. Puschnik, C. D. Marceau, L. Mlera, J. M. Grabowski, K. Kirkegaard, M. E. Bloom, P. Sarnow, C. R. Bertozzi, J. E. Carette, An RNA-centric dissection of host complexes controlling flavivirus infection. *Nat. Microbiol.* **4**, 2369–2382 (2019).
68. P. J. Murray, Macrophage polarization. *Annu. Rev. Physiol.* **79**, 541–566 (2017).
69. M. Benoit, B. Desnues, J.-L. Mege, Macrophage polarization in bacterial infections. *J. Immunol.* **181**, 3733–3739 (2008).
70. C. Zheng, Y. C. Ouyang, B. Jiang, X. Lin, J. Chen, M. Z. Dong, X. Zhuang, S. Yuan, Q. Y. Sun, C. Han, Non-canonical RNA polyadenylation polymerase FAM46C is essential for fastening sperm head and flagellum in mice. *Biol. Reprod.* **100**, 1673–1685 (2019).
71. T. Ganz, V. Gabayan, H.-I. Liao, L. Liu, A. Oren, T. Graf, A. M. Cole, Increased inflammation in lysozyme M-deficient mice in response to *Micrococcus luteus* and its peptidoglycan. *Blood* **101**, 2388–2392 (2003).
72. P. Markart, T. R. Korfhagen, T. E. Weaver, H. T. Akinbi, Mouse lysozyme M is important in pulmonary host defense against *Klebsiella pneumoniae* infection. *Am. J. Respir. Crit. Care Med.* **169**, 454–458 (2004).
73. H. T. Akinbi, R. Epaud, H. Bhatt, T. E. Weaver, Bacterial killing is enhanced by expression of lysozyme in the lungs of transgenic mice. *J. Immunol.* **165**, 5760–5766 (2000).
74. A. M. Cole, D. R. Thapa, V. Gabayan, H.-I. Liao, L. Liu, T. Ganz, Decreased clearance of *Pseudomonas aeruginosa* from airways of mice deficient in lysozyme M. *J. Leukoc. Biol.* **78**, 1081–1085 (2005).
75. E. del Cerro-Vadillo, F. Madrazo-Toca, E. Carrasco-Marín, L. Fernandez-Prieto, C. Beck, F. Leyva-Cobián, P. Saftig, C. Alvarez-Dominguez, Cutting edge: A novel nonoxidative phagosomal mechanism exerted by cathepsin-D controls *Listeria monocytogene*s intracellular growth. *J. Immunol.* **176**, 1321–1325 (2006).
76. Q. Fu, J. Yuan, L. Wang, H. Ran, F. Li, F. Liu, J. Zhang, W. Liu, W. Huang, Y. Huang, X. Xia, Proteomic analysis of murine macrophages mitochondria and lysosomes reveal Cathepsin D as a potential broad-spectrum antimicrobial protein. *J. Proteomics* **223**, 103821 (2020).
77. S.-D. Ha, A. Martins, K. Khazaie, J. Han, B. M. C. Chan, S. O. Kim, Cathepsin B is involved in the trafficking of TNF-α-containing vesicles to the plasma membrane in macrophages. *J. Immunol.* **181**, 690–697 (2008).
78. R. Elling, J. Chan, K. A. Fitzgerald, Emerging role of long noncoding RNAs as regulators of innate immune cell development and inflammatory gene expression. *Eur. J. Immunol.* **46**, 504–512 (2016).
79. M. K. Atianand, D. R. Caffrey, K. A. Fitzgerald, Immunobiology of long noncoding RNAs. *Annu. Rev. Immunol.* **35**, 177–198 (2017).
80. J. Blin, K. A. Fitzgerald, Perspective: The RNA exosome, cytokine gene regulation and links to autoimmunity. *Cytokine* **74**, 175–180 (2015).
81. C. Kew, W. Huang, J. Fischer, R. Ganesan, N. Robinson, A. Antebi, Evolutionarily conserved regulation of immunity by the splicing factor RNP-6/PUF60. *eLife* **9**, 1–23 (2020).
82. A. O. Olaitan, A. Aballay, Non-proteolytic activity of 19S proteasome subunit RPT-6 regulates GATA transcription during response to infection. *PLOS Genet.* **14**, e1007693 (2018).
83. V. Tiku, C. Kew, P. Mehrotra, R. Ganesan, N. Robinson, A. Antebi, Nucleolar fibrillarin is an evolutionarily conserved regulator of bacterial pathogen resistance. *Nat. Commun.* **9**, 1–10 (2018).
84. C.-W. Wu, K. Wimberly, A. Pietras, W. Dodd, M. B. Atlas, K. P. Choe, RNA processing errors triggered by cadmium and integrator complex disruption are signals for environmental stress. *BMC Biol.* **17**, 56 (2019).
85. R. Kaletsky, R. S. Moore, G. D. Vrla, L. R. Parsons, Z. Gitai, C. T. Murphy, *C. elegans* interprets bacterial non-coding RNAs to learn pathogenic avoidance. *Nature* **586**, 445–451 (2020).
86. B. A. Kudlow, L. Zhang, M. Han, Systematic analysis of tissue-restricted miRISCs reveals a broad role for microRNAs in suppressing basal activity of the *C. elegans* pathogen response. *Mol. Cell* **46**, 530–541 (2012).
87. Z. Ren, V. R. Ambros, *Caenorhabditis elegans* microRNAs of the let-7 family act in innate immune response circuits and confer robust developmental timing against pathogen stress. *Proc. Natl. Acad. Sci. U.S.A.* **112**, E2366–E2375 (2015).
88. L. Sun, L. Zhi, S. Shakoor, K. Liao, D. Wang, microRNAs involved in the control of innate immunity in Candida infected *Caenorhabditis elegans*. *Sci. Rep.* **6**, 36036 (2016).
89. J. Le Pen, H. Jiang, T. Di Domenico, E. Kneuss, J. Kosałka, C. Leung, M. Morgan, C. Much, K. L. M. Rudolph, A. J. Enright, D. O'Carroll, D. Wang, E. A. Miska, Terminal uridylyltransferases target RNA viruses as part of the innate immune system. *Nat. Struct. Mol. Biol.* **25**, 778–786 (2018).
90. C. E. Richardson, T. Kooistra, D. H. Kim, An essential role for XBP-1 in host protection against immune activation in *C. elegans*. *Nature* **463**, 1092–1095 (2010).
91. E. J. Tillman, C. E. Richardson, D. J. Cattie, K. C. Reddy, N. J. Lehrbach, R. Droste, G. Ruvkun, D. H. Kim, Endoplasmic reticulum homeostasis is modulated by the forkhead transcription factor FKH-9 during infection of *Caenorhabditis elegans*. *Genetics* **210**, 1329–1337 (2018).
92. E. Vidak, U. Javoršek, M. Vizovišek, B. Turk, Cysteine cathepsins and their extracellular roles: Shaping the microenvironment. *Cells* **8**, 264 (2019).
93. K. Lasocki, A. A. Bartosik, J. Mierzejewska, C. M. Thomas, G. Jagura-Burdzy, Deletion of the parA (soj) homologue in *Pseudomonas aeruginosa* causes ParB instability and affects growth rate, chromosome segregation, and motility. *J. Bacteriol.* **189**, 5762–5772 (2007).
94. A. Paix, A. Folkmann, D. Rasoloson, G. Seydoux, High efficiency, homology-directed genome editing in *Caenorhabditis elegans* using CRISPR-Cas9 ribonucleoprotein complexes. *Genetics* **201**, 47–54 (2015).

95. D. J. Dickinson, A. M. Pani, J. K. Heppert, C. D. Higgins, B. Goldstein, Streamlined genome engineering with a self-excising drug selection cassette. *Genetics* **200**, 1035–1049 (2015).
96. M. R. Green, J. Sambrook, *Molecular Cloning: A Laboratory Manual* (CSH Press, ed. 4, 2012).
97. J. Y. Jeong, H. S. Yim, J. Y. Ryu, H. S. Lee, J. H. Lee, D. S. Seen, S. G. Kang, One-step sequence-and ligation-independent cloning as a rapid and versatile cloning method for functional genomics Studies. *Appl. Environ. Microbiol.* **78**, 5440–5443 (2012).
98. M. Z. Li, S. J. Elledge, SLIC: A method for sequence- and ligation-independent cloning. *Methods Mol. Biol.* **852**, 51–59 (2012).
99. D. Graczyk, R. J. White, K. M. Ryan, Involvement of RNA polymerase III in immune responses. *Mol. Cell. Biol.* **35**, 1848–1859 (2015).
100. J. Pei, B. H. Kim, N. V. Grishin, PROMALS3D: A tool for multiple protein sequence and structure alignments. *Nucleic Acids Res.* **36**, 2295–2300 (2008).
101. R. C. Edgar, MUSCLE: A multiple sequence alignment method with reduced time and space complexity. *BMC Bioinformatics* **5**, 113 (2004).
102. I. Letunic, P. Bork, Interactive tree of life (iTOL) v4: Recent updates and new developments. *Nucleic Acids Res.* **47**, W256–W259 (2019).
103. J. Schindelin, I. Arganda-Carreras, E. Frise, V. Kaynig, M. Longair, T. Pietzsch, S. Preibisch, C. Rueden, S. Saalfeld, B. Schmid, J.-Y. Tinevez, D. J. White, V. Hartenstein, K. Eliceiri, P. Tomancak, A. Cardona, Fiji: An open-source platform for biological-image analysis. *Nat. Methods* **9**, 676–682 (2012).
104. M. Chekulaeva, H. Mathys, J. T. Zipprich, J. Attig, M. Colic, R. Parker, W. Filipowicz, miRNA repression involves GW182-mediated recruitment of CCR4-NOT through conserved W-containing motifs. *Nat. Struct. Mol. Biol.* **18**, 1218–1226 (2011).
105. M. Martin, Cutadapt removes adapter sequences from high-throughput sequencing reads. *EMBnet. J.* **17**, 10 (2011).
106. A. Dobin, C. A. Davis, F. Schlesinger, J. Drenkow, C. Zaleski, S. Jha, P. Batut, M. Chaisson, T. R. Gingeras, STAR: Ultrafast universal RNA-seq aligner. *Bioinformatics* **29**, 15–21 (2013).
107. Y. Liao, G. K. Smyth, W. Shi, FeatureCounts: An efficient general purpose program for assigning sequence reads to genomic features. *Bioinformatics* **30**, 923–930 (2014).
108. M. I. Love, W. Huber, S. Anders, Moderated estimation of fold change and dispersion for RNA-seq data with DESeq2. *Genome Biol.* **15**, 550 (2014).
109. D. Angeles-Albores, R. Y. Raymond, J. Chan, P. W. Sternberg, Tissue enrichment analysis for *C. elegans* genomics. *BMC Bioinformatics* **17**, 366 (2016).
110. A. D. Holdorf, D. P. Higgins, A. C. Hart, P. R. Boag, G. J. Pazour, A. J. M. Walhout, A. K. Walker, WormCat: An online tool for annotation and visualization of *Caenorhabditis elegans* genome-scale data. *Genetics* **214**, 279–294 (2020).
111. H. Li, Minimap2: Pairwise alignment for nucleotide sequences. *Bioinformatics* **34**, 3094–3100 (2018).
112. R. E. Workman, A. D. Tang, P. S. Tang, M. Jain, J. R. Tyson, R. Razaghi, P. C. Zuzarte, T. Gilpatrick, A. Payne, J. Quick, N. Sadowski, N. Holmes, J. G. de Jesus, K. L. Jones, C. M. Soulette, T. P. Snutch, N. Loman, B. Paten, M. Loose, J. T. Simpson, H. E. Olsen, A. N. Brooks, M. Akeson, W. Timp, Nanopore native RNA sequencing of a human poly(A) transcriptome. *Nat. Methods* **16**, 1–37 (2019).
113. U. Raudvere, L. Kolberg, I. Kuzmin, T. Arak, P. Adler, H. Peterson, J. Vilo, g:Profiler: A web server for functional enrichment analysis and conversions of gene lists (2019 update). *Nucleic Acids Res.* **47**, W191–W198 (2019).
114. A. R. Quinlan, I. M. Hall, BEDTools: A flexible suite of utilities for comparing genomic features. *Bioinformatics* **26**, 841–842 (2010).
115. J. R. Wiśniewski, P. Ostasiewicz, M. Mann, High recovery FASP applied to the proteomic analysis of microdissected formalin fixed paraffin embedded cancer tissues retrieves known colon cancer markers. *J. Proteome Res.* **10**, 3040–3049 (2011).
116. J. Cox, M. Mann, MaxQuant enables high peptide identification rates, individualized p.p.b.-range mass accuracies and proteome-wide protein quantification. *Nat. Biotechnol.* **26**, 1367–1372 (2008).
117. R Core Team, R: A language and environment for statistical computing (2020).
118. Y. Perez-Riverol, A. Csordas, J. Bai, M. Bernal-Llinares, S. Hewapathirana, D. J. Kundu, A. Inuganti, J. Griss, G. Mayer, M. Eisenacher, E. Pérez, J. Uszkoreit, J. Pfeuffer, T. Sachsenberg, Ş. Yilmaz, S. Tiwary, J. Cox, E. Audain, M. Walzer, A. F. Jarnuczak, T. Ternent, A. Brazma, J. A. Vizcaíno, The PRIDE database and related tools and resources in 2019: Improving support for quantification data. *Nucleic Acids Res.* **47**, D442–D450 (2019).
119. C. Frøkjaer-Jensen, M. W. Davis, C. E. Hopkins, B. J. Newman, J. M. Thummel, S.-P. Olesen, M. Grunnet, E. M. Jorgensen, Single-copy insertion of transgenes in *Caenorhabditis elegans*. *Nat. Genet.* **40**, 1375–1383 (2008).
120. D. J. Dickinson, J. D. Ward, D. J. Reiner, B. Goldstein, Engineering the *Caenorhabditis elegans* genome using Cas9-triggered homologous recombination. *Nat. Methods* **10**, 1028–1034 (2013).
121. G. J. Woodhead, C. A. Mutch, E. C. Olson, A. Chenn, Cell-autonomous β-catenin signaling regulates cortical precursor proliferation. *J. Neurosci.* **26**, 12620–12630 (2006).

Acknowledgments: We thank M. Krzyszton for helpful comments and the Dziembowski laboratory members for discussions. We are grateful to B. Goldstein, W. Filipowicz, D. Trono, and J. Jaworski for sharing plasmids; G. Jagura-Burdzy for sharing *P. aeruginosa* PAO1; D. Adamska for assistance with RNA-seq; O. Gewartowska, M. Szpila, E. Borsuk, and J. Gruchota for mice lines generation; and M. Hyjek-Składanowska for help with S200 chromatography. Some *C. elegans* strains were provided by the CGC, which is funded by NIH Office of Research Infrastructure Programs (P40 OD010440). **Funding:** This work was supported by National Science Center (OPUS 17 UMO-2019/33/B/NZ2/01773 to A.D., OPUS 14 UMO-2017/27/B/NZ2/01234 to S.M., and PRELUDIUM 19 UMO-2020/37/N/NZ2/02893 to A.B.). This research was supported by the funding from the European Union's Horizon 2020 research and innovation programme under grant agreement no 810425. A.B. was also supported by the Foundation for Polish Science (FNP). **Author contributions:** A.D. acquired funding and directed the studies. A.D., V.L., S.M., and A.B. designed the experiments. V.L. performed all *C. elegans* experiments and analyzed initial RNA-seq data. A.B. established primary BMDM cell cultures and performed all subsequent BMDM experiments. P.S.K. analyzed RNA-seq and *C. elegans* DRS data. S.M. performed tethering assays and preliminary BMDM experiments. N.G. analyzed BMDM DRS data. T.W. performed statistical colocalization analysis. D.C. analyzed MS data. Z.M. participated in *C. elegans* life span, CFU analysis, and transgenic strains generation. K.D. and J.J.E. contributed resources and helped to design experiments. V.L. and A.D. wrote the manuscript with input from P.S.K., A.B., and J.J.E. **Competing interests:** The authors declare that they have no competing interests. **Data and materials availability:** All data needed to evaluate the conclusions in the paper are present in the paper and/or the Supplementary Materials. RNA-seq data have been deposited to GEO database under the accession number GSE163549. Nanopore DRS data have been deposited to ENA with the following accession numbers: *C. elegans* and BMDM DRS, PRJEB40892; tethering experiment DRS, ERS12230818, ERS12230819, ERS12230820, and ERS6477295. Proteomics data have been deposited to the ProteomeXchange Consortium via the PRIDE (*118*) partner repository with identifier PXD023238. All plasmids and *C. elegans* strains generated in this study are available upon request from A.D. The mouse lines can be provided by A.D.'s pending scientific review and a completed material transfer agreement. Requests for the mice lines should be submitted to A.D.

Submitted 14 July 2022
Accepted 29 September 2022
Published 16 November 2022
10.1126/sciadv.add9468